

Differentially Private Federated Learning via Reconfigurable Intelligent Surface

Yuhan Yang, *Student Member, IEEE*, Yong Zhou, *Member, IEEE*, Youlong Wu *Member, IEEE*,
and Yuanming Shi, *Senior Member, IEEE*

Abstract—Federated learning (FL), as a disruptive machine learning paradigm, enables the collaborative training of a global model over decentralized local datasets without sharing them. It spans a wide scope of applications from Internet-of-Things (IoT) to biomedical engineering and drug discovery. To support low-latency and high-privacy FL over wireless networks, in this paper, we propose a reconfigurable intelligent surface (RIS) empowered over-the-air FL system to alleviate the dilemma between learning accuracy and privacy. This is achieved by simultaneously exploiting the channel propagation reconfigurability with RIS for boosting the receive signal power, as well as waveform superposition property with over-the-air computation (AirComp) for fast model aggregation. By considering a practical scenario where high-dimensional local model updates are transmitted across multiple communication blocks, we characterize the convergence behaviors of the differentially private federated optimization algorithm. We further formulate a system optimization problem to optimize the learning accuracy while satisfying privacy and power constraints via the joint design of transmit power, artificial noise, and phase shifts at RIS, for which a two-step alternating minimization framework is developed. Simulation results validate our systematic, theoretical, and algorithmic achievements and demonstrate that RIS can achieve a better trade-off between privacy and accuracy for over-the-air FL systems.

Index Terms—Federated learning, biomedical monitoring, reconfigurable intelligent surface, over-the-air computation, differential privacy.

I. INTRODUCTION

With the rapid advancement of communication technologies for Internet-of-Things (IoT), massive amounts of sensory data generated by various edge devices (e.g., smartphones, wearables) can be leveraged to support various intelligent applications and services [1]. However, the concern on data privacy makes the data sharing among edge devices unappealing and hinders the exploration of the potential values for the decentralized datasets. Recently, federated learning (FL) [2] has been recognized as a disruptive machine learning (ML) paradigm that is capable of preserving data privacy without sharing private raw data. FL spans a wide scope of applications from 6G [1], [3], [4], IoT [5], [6], and keyboard prediction [7], to the recent applications in healthcare informatics [8]–[10], medical imaging [11], drug discovery [12], and diabetes mellitus [13]. In particular, for cross-device FL, many edge devices collaboratively train a common model under the orchestration of a central edge server by periodically exchanging their local model updates. Despite the promising benefits, FL still

encounters many challenges including statistical heterogeneity, communication bottleneck, as well as privacy and security concerns [4], [14], [15].

The communication overhead incurred by the periodical model update exchange is a key performance-limiting factor of FL. To enable efficient model aggregation, over-the-air computation (AirComp) has been recently proposed as a promising aggregation scheme by integrating communication and computation [16]. Specifically, multiple edge devices can upload the local models concurrently by exploiting the waveform superposition property of a multiple-access channel [16]–[19], thereby achieving high spectrum efficiency and low transmission latency. In particular, AirComp was leveraged in [17] to reduce latency for FL over broadband channels compared with traditional orthogonal multiple access schemes. The learning performance of over-the-air FL was improved in [16] by jointly optimizing the receive beamforming design and device selection based on AirComp. The authors in [18] also proposed a gradient sparsification scheme for over-the-air stochastic gradient method to reduce the dimensionality of the exchanged updates.

Despite the aforementioned advantages, the heterogeneity of wireless links inevitably degrades the learning performance due to the magnitude attenuation and misalignment of signals received at the edge server. To alleviate the detrimental effect of wireless fading channels, reconfigurable intelligent surface (RIS) has recently been introduced as a key enabling technology to support fast and reliable model aggregation for over-the-air FL systems by reconfiguring the propagation environment [20]–[22]. Specifically, RIS is a planar metasurface equipped with an array of cost-effective passive reflecting elements, which are orchestrated by a software-enabled controller to adjust the phase shifts of the incident signals [23]–[26]. This helps improve the power of received signals, thereby enhancing the communication performance between all edge devices and the edge server. The waveform superposition property of a wireless multiple-access channel based on RIS is thus able to adapt to the local model updates, thereby improving the learning performance for over-the-air FL systems via jointly optimizing phase shifts, receive beamforming and edge device selection [21], [22].

Besides, as illustrated in [27]–[29], transmitting the model updates (e.g., local gradients) can still cause privacy leakage. To quantify the privacy disclosure, a rigorous mathematical framework called differential privacy (DP) [30], [31] has been proposed. Various privacy-preserving mechanisms have been developed by injecting random perturbations that obey specific

Y. Yang, Y. Zhou, Y. Wu, and Y. Shi are with ShanghaiTech University, Shanghai 201210, China (e-mail: {yangyh1, zhouyong, wuy11, shiyu}@shanghaitech.edu.cn).

Notation	Description	Notation	Description
K	Number of edge devices	N	Number of passive reflecting elements of RIS
D_k	Size of local dataset in the k -th edge device	T	Total number of learning rounds
e	Channel coherence length	I	Number of communication blocks in one learning round
θ	d -dimensional model parameter	(ϵ, δ)	Privacy level and failure probability
$\mathbf{g}_{k,t}$	Local update of edge device k in the t -th learning round	$\mathbf{n}_{k,t}(i)$	Artificial noise of edge device k in the i -th block
$\alpha_{k,t}(i)$	Transmit scalar of edge device k in the i -th block	$\eta_t(i)$	Uniform power scaling factor in the i -th block
$\mathbf{s}_{k,t}(i)$	Pre-processed signal of edge device k in the i -th block	$\mathbf{x}_{k,t}(i)$	Transmit signal of edge device k in the i -th block
$\mathbf{r}_t(i)$	Aggregated signal in the i -th block of learning round t	$\mathbf{w}_t(i)$	Additive white Gaussian noise in the i -th block
$h_{k,t}^d(i)$	Channel coefficient from edge device k to the edge server	$\mathbf{h}_{k,t}^r(i)$	Channel coefficient from edge device k to RIS
\mathbf{m}_t	Channel coefficient from RIS to the edge server	$h_{k,t}(i)$	Composite channel response of the k -th edge device
$\Theta_t(i)$	Phase shift matrix of RIS in the i -th block	P_0	Maximum transmit power of all edge devices
$\sigma_{k,t}^2(i)$	Power of artificial noise $\mathbf{n}_{k,t}(i)$	N_0	Power of wireless channel noise

TABLE I: Summary of notations in this paper.

distributions, e.g., Gaussian [30], Laplacian [32], and Binomial [33]. In particular, the authors in [34] developed an AirComp based FL scheme to achieve privacy protection for free. This procedure is accomplished by leveraging the inherent wireless channel noise to protect user privacy. The authors in [35] proved the inherent anonymity of AirComp which hides each private local update in the crowd to ensure high privacy, thereby reducing the amount of artificial noise added to the local updates. A disturbance scheme with additional perturbations added to a partial set of edge devices to benefit the whole system was proposed in [36]. However, the learning accuracy of FL may significantly degenerate due to the reduction of signal-to-noise ratio (SNR) for privacy guarantee [34], which yields a trade-off between accuracy and privacy.

To balance the privacy-accuracy trade-off, the existing works [34]–[38] only focus on designing power allocation schemes, without considering the reconfigurability of the wireless environment. In comparison, we propose an RIS-enabled over-the-air FL system to balance the trade-off between privacy and accuracy, which is achieved by simultaneously exploiting the channel propagation reconfigurability with RIS and waveform superposition property with AirComp. Besides, we consider a practical local model updates transmission scheme by distributing the high-dimensional model updates (e.g., deep neural network model) across multiple communication blocks in one learning round [39]. However, most of the previous works often make the lightweight assumption on the learning models, which requires the dimension of model updates to be small enough to be transmitted within one communication block [22], [34]–[38], [40], [41]. Through convergence analysis and system optimization, we reveal that the RIS-enabled FL system can enhance system SNR and boost the received signal power to establish high learning accuracy while satisfying the privacy requirements.

The major contributions of this paper are summarized as follows:

- From a systematic perspective, we develop an RIS-enabled FL system with privacy guarantees for fast and reliable model aggregation to alleviate the dilemma between learning accuracy and privacy by exploiting channel propagation reconfigurability and waveform superposition property.
- From a theoretical perspective, for high-dimensional model updates transmission across multiple communica-

tion blocks in one learning round, we propose a privacy-preserving transmission scheme based on DP and analyze its convergence behavior.

- From an algorithmic perspective, we propose a two-step alternating minimization framework to jointly optimize the transmit power, artificial noise, and phase shifts for system optimization, leading to an optimal power allocation scheme.
- Simulation results validate our systematic, theoretical, and algorithmic achievements and demonstrate the advantages of deploying RIS for enhancing both privacy and accuracy performance in the learning process.

The remainder of this paper is organized as follows. The privacy-preserving RIS-enabled FL system is presented in Section II. Section III analyzes the training loss, privacy, and power constraints, yielding a nonconvex system optimization problem. In Section IV, an alternating minimization framework is proposed for solving this nonconvex problem. Simulation results are elaborated in Section V to demonstrate the advantages of the RIS-enabled FL system. Finally, Section VI concludes this work.

Notations: Italic and boldface letters denote scalar and vector (matrix), respectively. $\mathbb{R}^{m \times n}$ and $\mathbb{C}^{m \times n}$ denote the real and complex domains with the space of $m \times n$, respectively. For a positive integer i , we let $[i] \triangleq \{1, \dots, i\}$. The operators $(\cdot)^T$, $(\cdot)^H$, $\text{Tr}(\cdot)$, $\text{rank}(\cdot)$, $\mathbb{E}(\cdot)$, and $\text{diag}(\cdot)$ represent the transpose, Hermitian transpose, trace, rank, statistical expectation, and diagonal matrix, respectively. \wedge denotes logical and operation. The operator $|\cdot|$ is the cardinality of a set or the absolute value of a scalar number, and $\|\cdot\|$ denotes the Euclidean norm.

II. SYSTEM MODEL

In this section, we first introduce an RIS-enabled FL system based on AirComp for fast and accurate model aggregation, followed by presenting a DP-based privacy-preserving pipeline for privacy concerns. The notations are listed in Table I.

A. Distributed Federated Learning

As shown in Fig. 1, we consider an RIS-enabled wireless FL system consisting of one single-antenna edge server, K single-antenna edge devices indexed by set $\mathcal{K} = \{1, \dots, K\}$, and an RIS equipped with N passive reflecting elements. We

assume that each edge device $k \in \mathcal{K}$ has its own local dataset \mathcal{D}_k with $D_k = |\mathcal{D}_k|$ data samples. For a given d -dimensional model parameter $\theta \in \mathbb{R}^d$, the local loss function of edge device k is defined as

$$F_k(\theta) = \frac{1}{D_k} \sum_{(\mathbf{x}, y) \in \mathcal{D}_k} f(\mathbf{x}, y; \theta), \quad (1)$$

where $f(\mathbf{x}, y; \theta)$ represents the sample-wise loss function quantifying the prediction error of model θ on training sample \mathbf{x} with respect to its true label y in \mathcal{D}_k . We assume that all local datasets have the same size [17], i.e., $D_k = D, \forall k \in \mathcal{K}$. Then, the global loss function can be defined as

$$F(\theta) = \frac{1}{\sum_{k=1}^K D_k} \sum_{k=1}^K D_k F_k(\theta) = \frac{1}{K} \sum_{k=1}^K F_k(\theta), \quad (2)$$

which refers to the empirical average of the sample-wise loss functions on the global dataset $\mathcal{D} = \bigcup_{k=1}^K \mathcal{D}_k$. We also assume that each edge device observes i.i.d. samples from a common distribution [34]. The non-i.i.d. setting in FL is also of special interest [42], but it is not the focus of this work.

The learning process minimizes (2) by updating θ based on the local gradients sent by edge devices, i.e.,

$$\theta^* = \underset{\theta \in \mathbb{R}^d}{\operatorname{argmin}} F(\theta). \quad (3)$$

This problem can be tackled by using the popular decentralized optimization method, e.g., **FedSGD** [2]. For analytical ease, in this paper, full-batch gradient descent is adopted for local model update and θ is updated periodically within T training rounds [16], [34], [38]. The t -th learning round consists of the following procedures:

- **Broadcast:** The edge server broadcasts the current global model parameter θ_t to all edge devices.
- **Local update:** Each edge device k computes its local update $\mathbf{g}_{k,t}$ with respect to its local dataset \mathcal{D}_k based on θ_t , i.e.,

$$\mathbf{g}_{k,t} = \nabla F_k(\theta_t) \in \mathbb{R}^d. \quad (4)$$

- **Model aggregation:** All edge devices in \mathcal{K} upload $\{\mathbf{g}_{k,t}\}$ to the edge server. Then the edge server updates θ_{t+1} based on the aggregated local updates via gradient descent, i.e.,

$$\theta_{t+1} = \theta_t - \lambda \hat{\mathbf{g}}_t, \quad (5)$$

where λ denotes the learning rate and $\hat{\mathbf{g}}_t$ is an estimation of the global gradient $\mathbf{g}_t = \nabla F(\theta_t) = \frac{1}{K} \sum_{k=1}^K \mathbf{g}_{k,t}$.

B. Channel Model for RIS-Enabled FL Systems

The existence of unfavorable channel propagations and the power limitation of each edge device may severely degrade the accuracy for model aggregation, thereby reducing the learning accuracy of the FL system. To address this issue, an RIS equipped with N reflecting elements is deployed to enhance the channel conditions of the channel links between all edge devices and the edge server [22].

We focus on the information exchange process among the edge server, RIS, and edge devices, as shown in Fig. 1. To simplify the theoretical analysis, the downlink channels

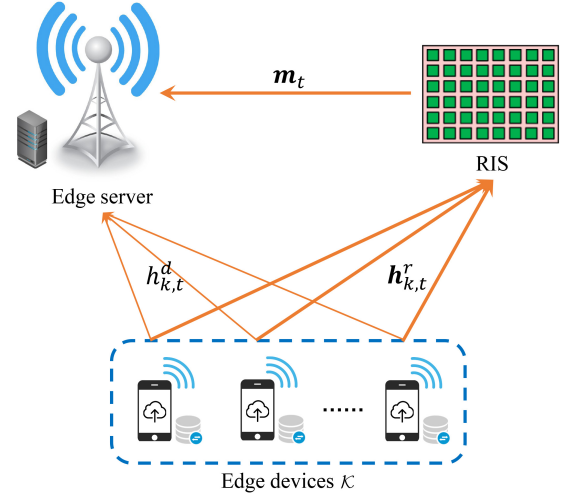


Fig. 1: An RIS-enabled wireless FL system.

are assumed to be noise-free [41], [43], while we mainly consider the uplink fading channels for aggregating the local models [21]. As the dimension d of the model parameters is often much larger than the channel coherence length e [39], we propose a practical transmission scheme illustrated in Fig. 2, where each edge device uploads its local update sequentially over several consecutive communication blocks. Specifically, in the t -th learning round, the whole update message $\mathbf{x}_{k,t} = [\mathbf{x}_{k,t}^T(1), \dots, \mathbf{x}_{k,t}^T(I)]^T \in \mathbb{C}^d$ (which will be elaborated in Section II-D) that is a function of $\mathbf{g}_{k,t}$ is evenly divided into $I = \lceil d/e \rceil$ e -dimensional vectors denoted by $\{\mathbf{x}_{k,t}(i) \in \mathbb{C}^e\}$. Then $\{\mathbf{x}_{k,t}(i)\}$ are sequentially transmitted across I communication blocks. We further assume $I = d/e$ for simplicity.

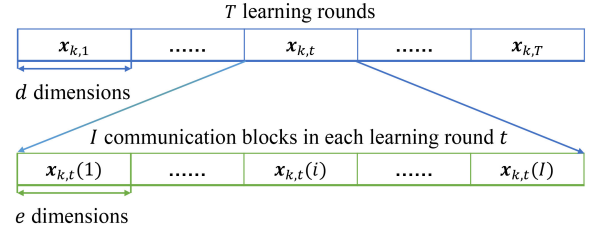


Fig. 2: The transmission process of edge device k , where one learning round contains I communication blocks.

For the i -th communication block in learning round t , let $h_{k,t}^d(i) \in \mathbb{C}$, $h_{k,t}^r(i) \in \mathbb{C}^N$, and $\mathbf{m}_t(i) \in \mathbb{C}^N$ denote the channel responses from edge device k to the edge server, from edge device k to RIS, and from RIS to the edge server, respectively. We assume that the channel coefficients are independent across different communication blocks and remain invariant during one communication block. We also assume that perfect channel state information (CSI) is available [21], [22], [43]. Moreover, the phase-shift matrix of the RIS is denoted as $\Theta_t(i) = \operatorname{diag}(\beta e^{j\phi_{1,t}(i)}, \dots, \beta e^{j\phi_{N,t}(i)}) \in \mathbb{C}^{N \times N}$, where $\phi_{n,t}(i) \in [0, 2\pi)$, $n \in \{1, \dots, N\}$. Without loss of generality, the amplitude reflection coefficient β at each reflecting element is set to be one [44]. We assume that $\Theta_t(i)$ is designed at the edge server and then transmitted to the RIS via error-free downlink channels. We also assume that signals reflected twice or more times by the RIS can be ignored [24]. The

composite channel response of the k -th edge device is thus denoted as $h_{k,t}(i) = \mathbf{m}_t^T(i)\Theta_t(i)\mathbf{h}_{k,t}^r(i) + h_{k,t}^d(i)$.

In the i -th communication block of learning round t , the aggregated signal at the edge server is given by

$$\mathbf{r}_t(i) = \sum_{k=1}^K h_{k,t}(i) \mathbf{x}_{k,t}(i) + \mathbf{w}_t(i), \quad (6)$$

where $\mathbf{w}_t(i) \sim \mathcal{CN}(\mathbf{0}, N_0 \mathbf{I}_e)$ is the additive white Gaussian noise (AWGN) and the aggregated signal $\mathbf{r}_t \in \mathbb{C}^d$ can be written as $\mathbf{r}_t = [\mathbf{r}_t^T(1), \dots, \mathbf{r}_t^T(I)]^T$ for the t -th learning round.

C. Differential Privacy

In the RIS-enabled FL system, the sensitive raw data never leaves the edge devices to protect users' privacy. Nevertheless, as revealed in [29], the transmission of model updates $\mathbf{g}_{k,t}$ may leak information about the local dataset statistically, which requires additional mechanisms to provide stronger privacy guarantees. We assume that the edge server is honest-but-curious [40], i.e., the edge server aims to infer the local information of each edge device based on the received signals $\mathbf{r} = \{\mathbf{r}_t\}_{t=1}^T$. We introduce DP based on the concept of neighboring datasets. Let $\mathcal{D}_k = \{\mathbf{x}_1, \dots, \mathbf{x}_n\} \in \mathcal{X}^n$ denote a dataset comprising n data points from \mathcal{X} . Two datasets $\mathcal{D}_k = \{\mathbf{x}_1, \dots, \mathbf{x}_n\}$ and $\mathcal{D}'_k = \{\mathbf{x}'_1, \dots, \mathbf{x}'_n\}$ with the same cardinality are neighboring if they differ only by one element, i.e., there exists an index $i \in [n]$ such that $\mathbf{x}_i \neq \mathbf{x}'_i$ and $\mathbf{x}_j = \mathbf{x}'_j$ for all $i \neq j$. We then present the following definition [30], [31] for DP.

Definition 1. Given $\epsilon > 0$, $0 \leq \delta \leq 1$, and an arbitrary protocol $\mathcal{M} : \mathcal{X}^n \rightarrow \mathcal{Y}$. For any two possible neighboring datasets $\mathcal{D}_k, \mathcal{D}'_k \in \mathcal{X}^n$ and any subset $\Lambda \subseteq \mathcal{Y}$, protocol \mathcal{M} is (ϵ, δ) -differentially private (in short, (ϵ, δ) -DP), if the following inequality holds:

$$\Pr[\mathcal{M}(\mathcal{D}_k) \in \Lambda] \leq e^\epsilon \Pr[\mathcal{M}(\mathcal{D}'_k) \in \Lambda] + \delta. \quad (7)$$

Note that the case of $\delta = 0$ is called pure ϵ -DP.

Specifically, for edge device k , we set the received signal \mathbf{r} as test variable to be the output of protocol \mathcal{M} . Based on this, (ϵ, δ) -DP guarantees that for any neighboring datasets \mathcal{D}_k and \mathcal{D}'_k , the differential privacy loss

$$\mathcal{L}_{\mathcal{D}_k, \mathcal{D}'_k}(\mathbf{r}) = \ln \frac{\Pr(\mathbf{r}|\mathcal{D}_k)}{\Pr(\mathbf{r}|\mathcal{D}'_k)}, \quad (8)$$

i.e., the log-likelihood ratio of the neighboring datasets \mathcal{D}_k and \mathcal{D}'_k satisfies

$$\Pr\left(|\mathcal{L}_{\mathcal{D}_k, \mathcal{D}'_k}(\mathbf{r})| \leq \epsilon\right) \geq 1 - \delta. \quad (9)$$

From (9), we can see that a lower ϵ yields a higher privacy guarantee for the FL system.

To achieve the privacy level ϵ , a common method is to add random perturbations to the signals. We thus uniformly assign the artificial noise $\mathbf{n}_{k,t} = [\mathbf{n}_{k,t}^T(1), \dots, \mathbf{n}_{k,t}^T(I)]^T \in \mathbb{C}^d$ with $\mathbf{n}_{k,t}(i) \sim \mathcal{CN}(\mathbf{0}, \sigma_{k,t}^2(i) \mathbf{I}_e)$ to each communication block in the t -th learning round, yielding a noisy version of the local

update $\mathbf{g}_{k,t}$. Therefore, the pre-processed transmit signal of edge device k is given as

$$\mathbf{s}_{k,t}(i) = D_k \mathbf{g}_{k,t}(i) + \mathbf{n}_{k,t}(i). \quad (10)$$

Notice that, for simplicity, we omit some procedures such as gradient clipping [45] which may preclude a large value of $D_k \mathbf{g}_{k,t}(i)$.

D. Model Aggregation via Over-the-Air Computation

We leverage AirComp for fast model aggregation by exploiting signal superposition of a wireless multiple-access channel [20]. In AirComp, all edge devices transmit their local updates $\{\mathbf{g}_{k,t}(i)\}_{k=1}^K$ synchronously using the same time-frequency resources in the communication block, thereby achieving high communication efficiency [16].

Motivated by [46], based on the perfect CSI of each edge device, we design the block-based uniform-forcing transmit signal $\mathbf{x}_{k,t}(i)$ in the i -th communication block of learning round t as follows:

$$\mathbf{x}_{k,t}(i) = \alpha_{k,t}(i) \mathbf{s}_{k,t}(i) = \sqrt{\eta_t(i)} \frac{(h_{k,t}(i))^H}{|h_{k,t}(i)|^2} \mathbf{s}_{k,t}(i), \quad (11)$$

where $\alpha_{k,t}(i) \in \mathbb{C}$ denotes the transmit scalar which is given by $\alpha_{k,t}(i) = \sqrt{\eta_t(i)}/h_{k,t}(i)$ and $\sqrt{\eta_t(i)} > 0$ is the uniform power scaling factor. Given a maximum transmit power $P_0 > 0$ for all edge devices, we have the following power constraints in each communication block

$$\mathbb{E}\left(\|\mathbf{x}_{k,t}(i)\|^2\right) = \mathbb{E}\left(\|\alpha_{k,t}(i)\mathbf{s}_{k,t}(i)\|^2\right) \leq P_0, \forall k, i, t \quad (12)$$

by taking the expectation over the additive Gaussian noise in (10). Note that, for each communication block, $\eta_t(i)$ and $\Theta_t(i)$ are elaborately designed by the edge server and broadcasted to the edge devices and RIS, which result in additional communication overheads.

Therefore, based on (10) and (11), the aggregated signal $\mathbf{r}_t(i)$ defined in (6) can be rewritten as

$$\mathbf{r}_t(i) = \sqrt{\eta_t(i)} \sum_{k=1}^K D_k \mathbf{g}_{k,t}(i) + \sqrt{\eta_t(i)} \sum_{k=1}^K \mathbf{n}_{k,t}(i) + \mathbf{w}_t(i). \quad (13)$$

Then, the edge server computes the estimated global update $\hat{\mathbf{g}}_t(i)$ by

$$\begin{aligned} \hat{\mathbf{g}}_t(i) &= \frac{1}{KD\sqrt{\eta_t(i)}} \text{Re}\{\mathbf{r}_t(i)\} \\ &= \mathbf{g}_t(i) + \frac{1}{KD} \sum_{k=1}^K \text{Re}\{\mathbf{n}_{k,t}(i)\} + \frac{\text{Re}\{\mathbf{w}_t(i)\}}{KD\sqrt{\eta_t(i)}}, \end{aligned} \quad (14)$$

where $\mathbf{g}_t(i) = \sum_{k=1}^K \mathbf{g}_{k,t}(i)/K$. After I rounds of model aggregation, the resulting $\hat{\mathbf{g}}_t = [\hat{\mathbf{g}}_t^T(1), \dots, \hat{\mathbf{g}}_t^T(I)]^T$ is an unbiased estimation of the true global gradient $\mathbf{g}_t = [\mathbf{g}_t^T(1), \dots, \mathbf{g}_t^T(I)]^T$. But the existence of the artificial noise and wireless channel noise leads to inevitable inaccuracy in $\hat{\mathbf{g}}_t$, which yields a trade-off between accuracy and privacy. In particular, the learning accuracy also depends on SNR, which is defined as the ratio of the maximum transmit power and the

noise power in one communication block, i.e.,

$$\text{SNR} = \frac{P_0}{e \times N_0}, \quad (15)$$

where $e \times N_0$ represents the channel noises power within one communication block.

Remark 1 (Symbol-level synchronization): Note that the AirComp-based aggregation rule relies on symbol-level synchronization among edge devices. To achieve this, a feasible technique is timing advance mechanism [47], which is widely used in 4G Long Term Evolution (LTE) and 5G New Radio (NR) systems. Specifically, consider the case when deploying AirComp in traditional Orthogonal Frequency Division Multiplexing (OFDM) systems, we note that 1 MHz synchronization bandwidth can limit the timing offset within 0.1 microseconds [48], which is shorter than the typical length of cyclic prefix (5 microseconds) in LTE systems. Thus, the symbol-level synchronization for AirComp is feasible.

Remark 2 (Limitation of uniform-forcing scalar): According to (11), channels inversion power control is adopted to achieve amplitude alignment at the edge server. However, due to the power constraint in (12), the uniform-forcing approach may be inefficient when some edge devices encounter deep fadings, which results in a small value of $\eta_t(i)$. To overcome this issue, we can adopt the truncated-channel-inversion scheme [17], which allocates power to an edge device only if its channel gain exceeds a hard threshold. Besides, the deployment of RIS can also alleviate deep fadings by reconfiguring the wireless environment, which is elaborated in Section IV-A.

E. Assumptions

We list several widely used assumptions [22], [49] for theoretical analysis of differentially private FL systems.

Assumption 1. (Strong convexity) The global loss function $F(\theta)$ is strongly convex with parameter μ , i.e.,

$$F(\theta) \geq F(\theta') + \nabla F(\theta')^T (\theta - \theta') + \frac{\mu}{2} \|\theta - \theta'\|^2, \quad \forall \theta, \theta'. \quad (16)$$

Assumption 2. (Smoothness) The global loss function $F(\theta)$ is Lipschitz continuous with parameter L , i.e.,

$$F(\theta) \leq F(\theta') + \nabla F(\theta')^T (\theta - \theta') + \frac{L}{2} \|\theta - \theta'\|^2, \quad \forall \theta, \theta',$$

which implies the following inequality:

$$\|\nabla F(\theta) - \nabla F(\theta')\| \leq L \|\theta - \theta'\|, \quad \forall \theta, \theta' \in \mathbb{R}^d.$$

Assumption 3. (Block gradient bound) In any learning round t , for any training data sample (\mathbf{x}, y) , the sample-wise loss function is upper bounded by a given constant γ_t , i.e.,

$$\|\nabla f(\mathbf{x}, y; \theta_t)\| \leq \gamma_t, \quad \forall t. \quad (17)$$

Based on triangular inequality, for edge device k , there always exists a constant $\zeta_{k,t}(i) \leq \gamma_t$ satisfying $\|\mathbf{g}_{k,t}(i)\| \leq \zeta_{k,t}(i)$.

III. PERFORMANCE ANALYSIS AND SYSTEM OPTIMIZATION

In this section, we shall analyze the convergence behavior of the RIS-enabled FL system and show the key component of

the privacy-preserving mechanism. We then provide the system optimization formulation to model the dilemma between privacy and accuracy.

A. Convergence Analysis

In the t -th learning round, the edge server updates the global model based on the received signal \mathbf{r}_t . However, the fading channels $\{h_{k,t}(i)\}$ as well as the artificial noise $\{\mathbf{n}_{k,t}(i)\}$ and AWGN $\{\mathbf{w}_t(i)\}$ may severely degrade the learning performance. To characterize the convergence behavior of the RIS-enabled FL system, we leverage the expected value of the gap between the optimal value F^* and the iteration value $F(\theta_t)$ to measure the distortion over T learning rounds, i.e., $\mathbb{E}[F(\theta_{T+1}) - F^*]$. Hence, given $\{\eta_t(i), \sigma_{k,t}(i)\}$, we bound the average optimality gap in the following theorem.

Theorem 1. Under Assumptions 1 and 2, given learning rate $\lambda = 1/L$, after T learning iterations, the averaged optimality gap is upper bounded as

$$\begin{aligned} \mathbb{E}[F(\theta_{T+1})] - F^* &\leq \left(1 - \frac{\mu}{L}\right)^T [F(\theta_1) - F^*] + \frac{1}{4L} \times \\ &\frac{e}{(KD)^2} \sum_{t=1}^T \left(1 - \frac{\mu}{L}\right)^{T-t} \left(\sum_{k=1}^K \sum_{i=1}^I \sigma_{k,t}^2(i) + \sum_{i=1}^I \frac{N_0}{\eta_t(i)} \right). \end{aligned} \quad (18)$$

Proof. Please refer to Appendix A. \square

According to **Theorem 1**, we observe that the average optimality gap $\mathbb{E}[F(\theta_{T+1}) - F^*]$ is upper bounded by two terms. The first term will converge to 0 as T goes to infinity, while the second term in terms of $\{\sigma_{k,t}(i), \eta_t(i)\}$ cannot vanish due to the added artificial noise and wireless channel noise in each communication block. Besides, (18) is also related to $\Theta_t(i)$ as the selection of $\eta_t(i)$ depends on $\Theta_t(i)$, which will be presented in **Theorem 3**.

B. Privacy-Preserving Mechanism

We develop a privacy-preserving scheme based on DP to alleviate privacy concerns for edge devices. We assume that $\{\eta_t(i), \sigma_{k,t}(i), \Theta_t(i)\}$ are fixed constants, as they do not reveal any information about the local datasets. Therefore, we only focus on the upload process from edge devices to the edge server. In the t -th learning round, for edge device k , the disclosed signals regarding its local dataset \mathcal{D}_k are $\{\mathbf{g}_{k,t}(i)\}$ across I blocks. We decouple the received signal $\mathbf{r}_t(i)$ as

$$\mathbf{r}_t(i) = \sqrt{\eta_t(i)} D_k \mathbf{g}_{k,t}(i) + \sqrt{\eta_t(i)} \sum_{j \neq k} D_j \mathbf{g}_{j,t}(i) + \mathbf{q}_t(i), \quad (19)$$

where

$$\mathbf{q}_t(i) = \sqrt{\eta_t(i)} \sum_{j=1}^K \mathbf{n}_{j,t}(i) + \mathbf{w}_t(i). \quad (20)$$

In (19), the first term is the disclosed signal concerning \mathcal{D}_k , the second term is independent of edge device k , and the third term $\mathbf{q}_t(i)$ is Gaussian noise. We observe that the privacy-preserving disturbance in (20) includes the added artificial noise and the inherent channel noise. Besides, all update messages, i.e., the first and second terms in (19), enjoy the

same privacy protection provided by $\mathbf{q}_t(i)$. For notational ease, let $\mathbf{q}_t = [\mathbf{q}_t^T(1), \dots, \mathbf{q}_t^T(I)]^T$ denote the effective noise to ensure privacy for the transmission of $\{\mathbf{g}_{j,t}\}_{j=1}^K$ in the t -th learning round.

For edge device k , its privacy level (ϵ, δ) depends on the sensitivity of the disclosed noise-free function regarding its local dataset. We first recall the definition of l_2 -sensitivity [30].

Definition 2. Let \mathcal{M} be an arbitrary mechanism on the transmitted signals. The l_2 -sensitivity Δ is defined as the maximum difference of the outputs from two neighboring datasets \mathcal{D}_k and \mathcal{D}'_k , i.e.,

$$\Delta = \max_{\mathcal{D}_k, \mathcal{D}'_k} \|\mathcal{M}(\mathcal{D}_k) - \mathcal{M}(\mathcal{D}'_k)\|_2. \quad (21)$$

Recalling that the first term in (19) is the only disclosed function concerning \mathcal{D}_k . Let $\mathbf{u}_{k,t}$ denote the difference between the outputs from two neighboring datasets \mathcal{D}_k and \mathcal{D}'_k , which is given by

$$\mathbf{u}_{k,t} = [h_{k,t}(1)\alpha_{k,t}(1)\Delta\mathbf{g}_{k,t}^T(1), \dots, h_{k,t}(I)\alpha_{k,t}(I)\Delta\mathbf{g}_{k,t}^T(I)]^T, \quad (22)$$

where

$$\Delta\mathbf{g}_{k,t}(i) = \sum_{(\mathbf{x}, y) \in \mathcal{D}_k} \nabla f_i(\mathbf{x}, y; \boldsymbol{\theta}_t) - \sum_{(\mathbf{x}, y) \in \mathcal{D}'_k} \nabla f_i(\mathbf{x}, y; \boldsymbol{\theta}_t)$$

with $\nabla f_i(\mathbf{x}, y; \boldsymbol{\theta}_t)$ denoting the $(i-1)e+1$ -th to ie -th elements in $\nabla f(\mathbf{x}, y; \boldsymbol{\theta}_t)$. Then the l_2 -sensitivity $\Delta_{k,t}$ of device k is

$$\Delta_{k,t} = \max_{\mathcal{D}_k, \mathcal{D}'_k} \|\mathbf{u}_{k,t}\|_2. \quad (23)$$

By using the triangular inequality and Assumption 3, we have

$$\Delta_{k,t} \leq 2\gamma_t \max_{i \in [I]} \sqrt{\eta_t(i)}. \quad (24)$$

Based on (24), the privacy constraint for all edge devices is given in the following theorem.

Theorem 2. For any fixed sequence of $\{\eta_t(i), \sigma_{k,t}(i)\}_{t=1}^T$, the RIS-enabled FL system satisfies (ϵ, δ) -DP if we have

$$\sum_{t=1}^T \frac{4\gamma_t^2}{\xi_t} \max_{i \in [I]} \{\eta_t(i)\} \leq \mathcal{R}_{dp}(\epsilon, \delta), \quad (25)$$

where

$$\xi_t \leq \eta_t(i) \sum_{k=1}^K \sigma_{k,t}^2(i) + N_0, \quad \forall i, t, \quad (26)$$

denotes a lower bound of the power of the effective noise $\mathbf{q}_t(i)$, and $\mathcal{R}_{dp}(\epsilon, \delta) = (\sqrt{\epsilon + [C^{-1}(1/\delta)]^2} - C^{-1}(1/\delta))^2$ with $C^{-1}(x)$ denoting the inverse function of $C(x) = \sqrt{\pi}xe^{x^2}$.

Proof. Please refer to Appendix B. \square

From **Theorem 2**, we emphasize that both the artificial noise and the receiver noise contribute to the privacy guarantee. Besides, based on (26), ξ_t represents a lower bound of the weakest privacy-preserving perturbation (i.e., the lowest effective noise power) across I communication blocks in the t -th learning round. Furthermore, the privacy guarantee is related to the joint effect of ξ_t and the maximum transmit power scalar $\eta_t(i)$ among I communication blocks. We also notice that the

relationship between the privacy constraint and the phase-shift matrix $\boldsymbol{\Theta}_t(i)$ is similar to **Theorem 1**.

C. System Optimization

To design the RIS-enabled FL system, we shall propose to minimize the optimality gap in (18) while satisfying the privacy and the maximum transmit power constraints given in (25) and (12), respectively, across T learning rounds. Specifically, given the privacy level (ϵ, δ) , we jointly optimize $\{\sigma_{k,t}(i), \boldsymbol{\Theta}_t(i), \eta_t(i), \xi_t\}$ in each communication block. Based on (10), (11) and (12), we obtain the power constraints,

$$\mathbb{E} \left(\|\mathbf{x}_{k,t}\|^2 \right) \stackrel{(a)}{\leq} \frac{\eta_t(i)}{|h_{k,t}(i)|^2} [D_k^2 \zeta_{k,t}^2(i) + e\sigma_{k,t}^2(i)] \leq P_0, \quad \forall i, k, t,$$

where (a) comes from the fact $\|\mathbf{g}_{k,t}(i)\| \leq \zeta_{k,t}(i)$ in Assumption 3, along with the triangular inequality.

Note that, the optimization variables are only related to the second term in (18). We obtain the following optimization problem \mathcal{P} :

$$\begin{aligned} & \underset{\{\eta_t, \xi_t, \boldsymbol{\Theta}_t, \sigma_{k,t}\}}{\text{minimize}} && \sum_{t=1}^T \left(1 - \frac{\mu}{L}\right)^{-t} \left(\sum_{k=1}^K \sum_{i=1}^I \sigma_{k,t}^2(i) + \sum_{i=1}^I \frac{N_0}{\eta_t(i)} \right) \end{aligned} \quad (27a)$$

$$\text{subject to} \quad \sum_{t=1}^T \frac{4\gamma_t^2}{\xi_t} \max_{i \in [I]} \{\eta_t(i)\} \leq \mathcal{R}_{dp}(\epsilon, \delta), \quad (27b)$$

$$\xi_t \leq \eta_t(i) \sum_{k=1}^K \sigma_{k,t}^2(i) + N_0, \quad \forall i, t, \quad (27c)$$

$$\frac{\eta_t(i)}{|\mathbf{m}_t^T(i)\boldsymbol{\Theta}_t(i)\mathbf{h}_{k,t}^r(i) + h_{k,t}^d(i)|^2} [D_k^2 \zeta_{k,t}^2(i) + e\sigma_{k,t}^2(i)] \leq P_0, \quad \forall i, k, t, \quad (27d)$$

$$|\boldsymbol{\Theta}_t(i)(n, n)| = 1, \quad \forall i, n, t, \quad (27e)$$

where (27b) and (27c) denote the privacy constraints for all edge devices as presented in (25) and (26), respectively, (27d) represents the power constraints by substituting $h_{k,t}(i) = \mathbf{m}_t^T(i)\boldsymbol{\Theta}_t(i)\mathbf{h}_{k,t}^r(i) + h_{k,t}^d(i)$ into (12), and (27e) indicates the unit modulus constraints of all reflecting elements at RIS with $\boldsymbol{\Theta}_t(i)(n, n)$ denoting as the (n, n) -th entry of $\boldsymbol{\Theta}_t(i)$. Unfortunately, due to the non-convexity of the privacy and power constraints, and the nonconvex unimodular constraints of the phase shifts at RIS, problem \mathcal{P} is highly intractable and computationally challenging.

IV. A TWO-STEP ALTERNATING LOW-RANK OPTIMIZATION FRAMEWORK

In this section, we propose a two-step alternating minimization framework for solving problem \mathcal{P} . Specifically, the transmit power scalar $\eta_t(i)$ and artificial noise $\sigma_{k,t}(i)$ at each edge device, as well as the phase-shift matrix $\boldsymbol{\Theta}_t(i)$ at the RIS are optimized in an alternative manner until the algorithm converges.

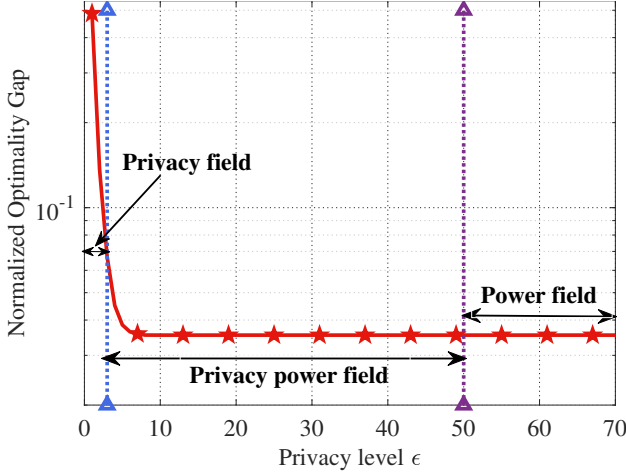


Fig. 3: The relationship between learning accuracy and privacy level. The two vertical lines distinguish different cases.

A. Co-Design of Artificial Noise and Power Scalar

The main idea of this framework is to alternately optimize $\{\eta_t(i), \sigma_{k,t}(i), \Theta_t(i), \xi_t\}$ in T learning rounds. Note that problem \mathcal{P} is a non-causal setting where parameters $\{h_{k,t}^r(i), m_t(i), h_{k,t}^d(i), \zeta_{k,t}(i), \gamma_t\}$ need to be known in advance, which will be discussed in Section VI-C.

Given the phase-shift matrix $\Theta_t(i)$, problem \mathcal{P} is reduced to problem \mathcal{P}_1 as follows:

$$\text{minimize}_{\{\eta_t, \sigma_{k,t}, \xi_t\}} \sum_{t=1}^T \left(1 - \frac{\mu}{L}\right)^{-t} \left(\sum_{k=1}^K \sum_{i=1}^I \sigma_{k,t}^2(i) + \sum_{i=1}^I \frac{N_0}{\eta_t(i)} \right) \quad (28a)$$

$$\text{subject to} \quad \sum_{t=1}^T \frac{4\gamma_t^2}{\xi_t} \max_{i \in [I]} \{\eta_t(i)\} \leq \mathcal{R}_{dp}(\epsilon, \delta), \quad (28b)$$

$$\xi_t \leq \eta_t(i) \sum_{k=1}^K \sigma_{k,t}^2(i) + N_0, \quad \forall i, t, \quad (28c)$$

$$\frac{D^2 \zeta_{k,t}^2(i) + e \sigma_{k,t}^2(i)}{|h_{k,t}(i)|^2} \eta_t(i) \leq P_0, \quad \forall i, k, t, \quad (28d)$$

where $h_{k,t}(i) = m_t^T(i) \Theta_t(i) h_{k,t}^r(i) + h_{k,t}^d(i)$ denotes the composite channel response which remains constant given $\Theta_t(i)$. We note that through a change of variables, problem \mathcal{P}_1 can be transformed into a convex problem tackled by KKT conditions, leading to an adaptative power allocation mechanism, i.e., **Theorem 3**. For analytical ease, we denote τ_t as the number of communication blocks which are restricted by privacy in the t -th learning round.

Theorem 3. The optimal solution to problem \mathcal{P}_1 is given by

$$\xi_t = N_0, \quad \forall t, \quad \sigma_{k,t}(i) = 0, \quad \forall i, k, t, \quad (29)$$

and the selection of $\{\eta_t(i)\}$ depends on the joint effect of privacy and power, which yields the following three cases:

- (a) **Privacy field:** If $\tau_t = I$ for all learning rounds, then the optimal $\{\eta_t(i)\}_{i=1}^I$ remains a constant η_t with

$$\eta_t = \frac{N_0 \sqrt{I}}{2\gamma_t \beta^{\frac{1}{2}}} \left(1 - \frac{\mu}{L}\right)^{-\frac{1}{2}} \wedge \eta_t < P_0 \min_{i,k} \frac{|h_{k,t}(i)|^2}{D^2 \zeta_{k,t}^2(i)}, \quad (30)$$

Power alignment for each edge device in the t -th learning round ($K = 5, I = 5$)

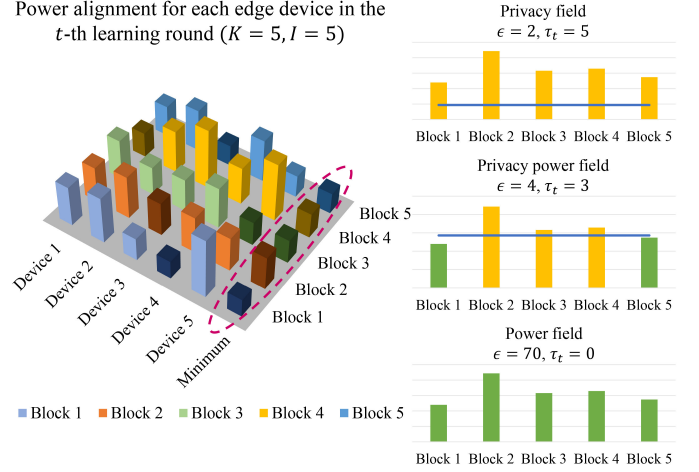


Fig. 4: Power allocation under different privacy levels in one learning round. The blue lines indicate the privacy limitations.

where β is selected to strictly satisfy (28b), i.e.,

$$\sum_{t=1}^T \frac{4\gamma_t^2}{N_0} \eta_t = \sum_{t=1}^T \frac{2\sqrt{I}\gamma_t}{\beta^{\frac{1}{2}}} \left(1 - \frac{\mu}{L}\right)^{-\frac{1}{2}} = \mathcal{R}_{dp}(\epsilon, \delta). \quad (31)$$

- (b) **Privacy power field:** It is a generalized version of (a) with $\tau_t \in [I]$, and the optimal $\eta_t(i)$ is given by

$$\eta_t(i) = \min \left\{ \frac{N_0 \sqrt{\tau_t}}{2\gamma_t \beta^{\frac{1}{2}}} \left(1 - \frac{\mu}{L}\right)^{-\frac{1}{2}}, P_0 \min_k \frac{|h_{k,t}(i)|^2}{D^2 \zeta_{k,t}^2(i)} \right\}, \quad (32)$$

where β and τ_t are selected to strictly satisfy (28b), i.e.,

$$\sum_{t=1}^T \frac{4\gamma_t^2}{N_0} \max_{i \in [I]} \{\eta_t(i)\} = \sum_{t=1}^T \frac{4\gamma_t^2}{N_0} \min_{i \in [I]} \left\{ \frac{N_0 \sqrt{\tau_t}}{2\gamma_t \beta^{\frac{1}{2}}} \left(1 - \frac{\mu}{L}\right)^{-\frac{1}{2}}, P_0 \max_{i \in [I]} \left\{ \min_{k \in [K]} \frac{|h_{k,t}(i)|^2}{D^2 \zeta_{k,t}^2(i)} \right\} \right\} = \mathcal{R}_{dp}(\epsilon, \delta).$$

- (c) **Power field:** If $\tau_t = 0$ holds for all learning rounds, i.e.,

$$\sum_{t=1}^T \frac{4P_0 \gamma_t^2}{N_0} \max_{i \in [I]} \left\{ \min_{k \in [K]} \frac{|h_{k,t}(i)|^2}{D^2 \zeta_{k,t}^2(i)} \right\} < \mathcal{R}_{dp}(\epsilon, \delta), \quad (33)$$

the unique optimal power scalar $\eta_t(i)$ is given by

$$\eta_t(i) = P_0 \min_{k \in [K]} \frac{|h_{k,t}(i)|^2}{D^2 \zeta_{k,t}^2(i)}. \quad (34)$$

Proof. Please refer to Appendix C. \square

From **Theorem 3**, the power of artificial noise becomes zero, which indicates that the additive channel noise in model aggregation serves as an inherent privacy-preserving mechanism to guarantee DP levels for each edge device [34]. Besides, as shown in Fig. 3, three cases characterize the learning accuracy of the FL system. Essentially, the power allocation scheme, i.e., the selection of $\eta_t(i)$ under different ϵ causes the difference in learning accuracy. To make it precise, Fig. 4 illustrates this process in one learning round. Specifically, two power alignment schemes are developed for comparison, where one represents the maximum transmit power concerning privacy requirement $\{\epsilon, \tau_t\}$, and the other indicates the case

without privacy, i.e., the Minimum column in Fig. 4. We note that τ_t , which represents the impact of ϵ across I communication blocks, is the key component of **Theorem 3**. Concretely, τ_t indicates the number of communication blocks restricted by privacy in one learning round, i.e., the number of yellow bars in Fig. 4. Consequently, different ϵ results in a different selection of τ_t , yielding the following three cases:

- Case (a): Due to the extremely strict privacy level, all communication blocks in this case are restricted by privacy, i.e., $\tau_t = I$.
- Case (b): In this case, several communication blocks are restricted by privacy while others are limited by transmit power, i.e., $\tau_t \in [I]$. Besides, cases (a) and (b) must satisfy the equality in (27b), which is achieved by adaptively selecting $\{\beta, \tau_t\}$ through enumeration.
- Case (c): In this case, due to the quite loose privacy level, all communication blocks are limited by the transmit power constraints, i.e., $\tau_t = 0$.

We reveal the benefits achieved by RIS to the above three cases. Due to the reconfigurable capability of RIS, we note that the RIS-enabled FL system is able to establish better channel conditions compared to the FL systems without RIS. Besides, according to (32) and (34), the RIS-enabled FL system can enjoy higher transmit power and enhance the power of received signals at the edge server, thereby resulting in high learning accuracy. However, when the privacy level is strict, i.e., Case (a), the learning accuracy is restricted by privacy and cannot be improved by RIS. We will further explore the significant impacts brought by RIS on the learning accuracy via simulations in Section V.

B. Design of Phase-Shift Matrix

On the other hand, for given the artificial noise and power scalar $\{\sigma_{k,t}(i), \eta_t(i)\}$, problem \mathcal{P} becomes the following nonconvex feasibility detection problem \mathcal{P}_2 :

$$\text{find } \Theta_t(i) \quad (35a)$$

$$\text{subject to } \frac{\eta_t(i) D^2 \zeta_{k,t}^2(i)}{|\mathbf{m}_t^T(i) \Theta_t(i) \mathbf{h}_{k,t}^r(i) + h_{k,t}^d(i)|^2} \leq P_0, \forall i, k, t, \quad (35b)$$

$$|\Theta_t(i)(n, n)| = 1, \forall i, n, t. \quad (35c)$$

For analytical ease, by denoting $v_{n,t}(i) = e^{j\phi_{n,t}(i)}$ and $\mathbf{c}_{k,t}^H(i) = \mathbf{m}_t^T(i) \text{diag}(\mathbf{h}_{k,t}^r(i))$, we have $\mathbf{m}_t^T(i) \Theta_t(i) \mathbf{h}_{k,t}^r(i) = \mathbf{c}_{k,t}^H(i) \mathbf{v}_t(i)$, where $\mathbf{v}_t(i) = [v_{1,t}(i), \dots, v_{N,t}(i)]^T$. Therefore, problem (35) is further transformed into problem $\mathcal{P}_{2.1}$:

$$\text{find } \mathbf{v}_t(i) \quad (36a)$$

$$\text{subject to } \frac{\eta_t(i) D^2 \zeta_{k,t}^2(i)}{|\mathbf{c}_{k,t}^H(i) \mathbf{v}_t(i) + h_{k,t}^d(i)|^2} \leq P_0, \forall k, t, \quad (36b)$$

$$|v_{n,t}(i)| = 1, \forall n \in [N]. \quad (36c)$$

Nevertheless, problem $\mathcal{P}_{2.1}$ is still nonconvex and inhomogeneous. To develop an efficient algorithm, by introducing an auxiliary variable $\iota_t(i)$, problem (36) can be equivalently reformulated as a homogeneous nonconvex quadratically con-

strained quadratic programming (QCQP) problem [24], [50], which is given by the following problem $\mathcal{P}_{2.2}$:

$$\text{find } \hat{\mathbf{v}}_t(i) \quad (37a)$$

$$\text{subject to } \hat{\mathbf{v}}_t^H(i) \mathbf{R}_{k,t}(i) \hat{\mathbf{v}}_t(i) + |h_{k,t}^d(i)|^2 \geq \eta_t(i) D^2 \zeta_{k,t}^2(i) / P_0, \forall i, k, t, \quad (37b)$$

$$|\hat{v}_{n,t}(i)| = 1, \forall n \in [N+1], \quad (37c)$$

where

$$\mathbf{R}_{k,t}(i) = \begin{bmatrix} \mathbf{c}_{k,t}(i) (\mathbf{c}_{k,t}(i))^H & \mathbf{c}_{k,t}(i) h_{k,t}^d(i) \\ (\mathbf{c}_{k,t}(i) h_{k,t}^d(i))^H & 0 \end{bmatrix}, \quad \hat{\mathbf{v}}_t(i) = \begin{bmatrix} \mathbf{v}_t(i) \\ \iota_t(i) \end{bmatrix}.$$

Let $\hat{\mathbf{v}}_t^*(i) = [\tilde{\mathbf{v}}_t^*(i)^T, \iota_t^*(i)]^T$ denote a feasible $\hat{\mathbf{v}}_t(i)$ to problem (37). Then a feasible solution $\mathbf{v}_t^*(i)$ to problem (36) can be immediately recovered by setting $\mathbf{v}_t^*(i) = \tilde{\mathbf{v}}_t^*(i) / \iota_t^*(i)$. A feasible solution $\Theta_t^*(i)$ to problem (35) can thus be expressed as $\Theta_t^*(i) = \text{diag}(\mathbf{v}_t^*(i))$.

To solve problem (37), a natural method is to formulate it as a semi-definite programming (SDP) problem by matrix lifting [16], [51]. Since $\hat{\mathbf{v}}_t^H(i) \mathbf{R}_{k,t}(i) \hat{\mathbf{v}}_t(i) = \text{Tr}(\mathbf{R}_{k,t}(i) \hat{\mathbf{v}}_t(i) \hat{\mathbf{v}}_t^H(i))$, we denote $\mathbf{V}_t(i)$ as the lifting matrix of $\hat{\mathbf{v}}_t(i)$, where $\mathbf{V}_t(i) = \hat{\mathbf{v}}_t(i) \hat{\mathbf{v}}_t^H(i)$ and $\text{rank}(\mathbf{V}_t(i)) = 1$. Therefore, problem $\mathcal{P}_{2.1}$ can be further transformed into the following problem $\mathcal{P}_{2.3}$:

$$\text{find } \mathbf{V}_t(i) \quad (38a)$$

$$\text{subject to } \text{Tr}(\mathbf{R}_{k,t}(i) \mathbf{V}_t(i)) + |h_{k,t}^d(i)|^2 \geq \eta_t(i) D^2 \zeta_{k,t}^2(i) / P_0, \forall i, k, t, \quad (38b)$$

$$\mathbf{V}_t(i)(n, n) = 1, \forall n \in [N+1], \quad (38c)$$

$$\text{rank}(\mathbf{V}_t(i)) = 1, \forall i, t, \quad (38d)$$

$$\mathbf{V}_t(i) \geq \mathbf{0}, \forall i, t, \quad (38e)$$

where $\mathbf{V}_t(i)(n, n)$ denotes the (n, n) -entry of matrix $\mathbf{V}_t(i)$.

However, the resulting problem $\mathcal{P}_{2.3}$ is still nonconvex due to the rank-one constraints in (38d). Fortunately, a feasible solution to this problem can be generated by simply dropping the rank-one constraints via the SDR technique [51]. The resulting SDP problem can be solved efficiently by existing convex optimization solvers such as CVX [52]. Although the Gaussian randomization technique in SDR may generate a suboptimal solution, we can still observe that a significant learning performance gain of the RIS-enabled FL system can be achieved through numerical experiments.

Without causing confusion, we omit parameter i for notational ease, e.g., $\Theta_t(i)$ as Θ_t . We present the two-step iterative framework in **Algorithm 1** for solving problem \mathcal{P} . The computational cost of the proposed algorithm consists of solving a sequence of search programs for \mathcal{P}_1 and SDR programs [51] for \mathcal{P}_2 . From the complexity analysis of typical interior-point method, the worst-case complexity of **Algorithm 1** is obtained as $\mathcal{O}\left(JIT \max\{K, N+1\}^4 \sqrt{N+1} \log_2(1/o)\right)$, where $o > 0$ denotes the solution accuracy of SDR.

C. Discussion on the Causal Approximation

Based on the above observations, **Algorithm 1** solves the nonconvex problem \mathcal{P} with the knowledge of all channel re-

Algorithm 1: Two-step alternating minimization for solving problem \mathcal{P} (27) in the RIS-enabled FL system.

Input: The phase-shift matrix Θ_0 , the privacy level (ϵ, δ) , and the maximum iteration number J .

Initialize $j \leftarrow 1$ to denote the number of iterations.

repeat

 Given Θ_{j-1} , obtain solution $(\eta_j, \sigma_{k,j})$ by solving problem \mathcal{P}_1 (28).

 Given $(\eta_j, \sigma_{k,j})$, obtain solution Θ_j by solving problem \mathcal{P}_2 (35).

 Update $j \leftarrow j + 1$.

until (27a) is below a given threshold or $j > J$;

Output: $\eta_t(i) \leftarrow \eta_j$, $\Theta_t(i) \leftarrow \Theta_j$, $\sigma_{k,t}(i) \leftarrow \sigma_{k,j}$.

sponses $\{h_{k,t}^d(i), \mathbf{m}_t(i), \mathbf{h}_{k,t}^r(i)\}$ and local gradient information $\{\zeta_{k,t}(i), \gamma_t\}$, yielding an impractical non-causal system. We thus present some feasible prediction methods to approximate this non-causal system.

At the beginning of the training process, we need to address the following two questions for our proposed scheme:

- How to approximate the future gradient information?
- How to predict the future channel responses?

The first question aims at providing upper bounds for the L_2 -sensitivity defined in (23) and the local gradients. To this end, there exist multiple adaptive methods for practical use, such as the L -Lipschitz based technique [53], [54], and the adaptive clipping method [55] with a well-designed critical threshold based on the current gradients.

For the second question, this is essentially related to wireless channel prediction. To estimate channels accurately, many promising methods have been proposed. For instance, the authors in [34] specialized an accumulated mechanism where the future channel responses are assumed to be consistent with the current ones. But this assumption fails to exploit the correlation among channel blocks. To explore the inherent relationship between each communication block, several prediction techniques have been developed in [56], [57], including the Gauss-Markov process channel modeling method [58] and Wiener or Kalman filtering based approach [58], [59]. Besides, the deep learning methods turn out to be powerful to improve channel prediction accuracy [60]–[62]. We thus leave the design of effective casual models as our future work.

V. SIMULATION RESULTS

In this section, we present the simulation results to demonstrate the advantages of the RIS-enabled FL systems. Besides, the effectiveness of our proposed two-step alternating minimization framework will also be illustrated. Simulations are conducted using Matlab R2021b and the code is available at https://github.com/MengCongWo/FL_Privacy_blockcrossing.

A. Simulation Settings

We propose to gain insights into the impact of deploying RIS on learning accuracy based on ridge regression, whose

sample-wise loss function is given as

$$f(\mathbf{x}, y; \boldsymbol{\theta}) = \frac{1}{2} \|\boldsymbol{\theta}^T \mathbf{x} - y\|^2 + \nu \|\boldsymbol{\theta}\|^2, \quad (39)$$

where $\nu = 5 \times 10^{-5}$ denotes penalty coefficient. We randomly generate a dataset of scale $|\mathcal{D}| = 10^4$ and set the model dimension d to be 10. Specifically, the training samples \mathbf{x} are drawn i.i.d. according to $\mathcal{N}(\mathbf{0}, \mathbf{I}_d)$ while the corresponding true label y is given by $y = \mathbf{x}(2) + 3\mathbf{x}(5) + 0.2z_0$, where the data noise z_0 is drawn i.i.d. from $\mathcal{N}(0, 1)$. We uniformly divide the total dataset \mathcal{D} into K local datasets, and let the ratio

$$r = \max_{k \in [K]} \frac{|\mathcal{D}_k|}{|\mathcal{D}|} \in [0.1, 1) \quad (40)$$

denote the system heterogeneity representing various storage capacities of the edge devices and larger r yields higher heterogeneity. The global loss function F is μ -strongly convex, L -Lipschitz smooth and differentiable, where μ and L are specified by the smallest and largest eigenvalues of the data Gramian matrix $\mathbf{X}^T \mathbf{X} / D + 2\nu \mathbf{I}_d$ with the data matrix $\mathbf{X} = [\mathbf{x}_1, \dots, \mathbf{x}_D]$. Besides, the optimal $\boldsymbol{\theta}^*$ of (39) is $\boldsymbol{\theta}^* = (\mathbf{X}^T \mathbf{X} + 2D\nu \mathbf{I}_d)^{-1} \mathbf{X}^T \mathbf{y}$ with true label vector $\mathbf{y} = [y_1, \dots, y_D]^T$. As for the definitions of γ_t and $\zeta_{k,t}(i)$, we use the simple upper bounds as in [34, Section V-A]. Furthermore, we use the normalized optimality gap defined as $[F(\boldsymbol{\theta}_{T+1}) - F(\boldsymbol{\theta}^*)] / F(\boldsymbol{\theta}^*)$ to measure the learning accuracy.

The wireless channels are assumed to suffer from Rice fading [24], and the channel coefficients are given by

$$\boldsymbol{\varrho} = \sqrt{\frac{\kappa}{1+\kappa}} \boldsymbol{\varrho}_{LoS} + \sqrt{\frac{1}{1+\kappa}} \boldsymbol{\varrho}_{NLoS}, \quad (41)$$

where κ represents the Rician factor, $\boldsymbol{\varrho}_{LoS}$ denotes the deterministic line-of-sight (LoS) component, and $\boldsymbol{\varrho}_{NLoS}$ denotes the non-line-of-sight (NLoS) component. For simplicity, we set $\boldsymbol{\varrho}_{LoS} = 1$ and generate $\boldsymbol{\varrho}_{NLoS}$ by autoregressive (AR) scheme, which is defined as

$$\boldsymbol{\varrho}_{NLoS}(i) = \rho \boldsymbol{\varrho}_{NLoS}(i-1) + \sqrt{1 - \rho^2} \boldsymbol{\vartheta}(i), \quad (42)$$

where ρ denotes the correlation coefficient and $\boldsymbol{\vartheta}(i)$ is drawn based on an innovation process satisfying $\boldsymbol{\vartheta}(i) \sim \mathcal{N}(\mathbf{0}, \mathbf{I})$. Hence, the channel coefficients in the i -th communication block of learning round t are given by $\mathbf{m}_t(i) = \boldsymbol{\varrho}_{IB}$, $\mathbf{h}_{k,t}^r(i) = \boldsymbol{\varrho}_{DI}$, and $h_{k,t}^d(i) = \boldsymbol{\varrho}_{DB}$, whose Rician factors are given by κ_{IB} , κ_{DI} , and κ_{DB} , respectively. The parameter ρ is set to 1 for simplicity since ρ has no discernible effect on the performance in the case where perfect CSI is available for all edge devices.

Under the above simulation settings, we mainly compare the learning accuracy under the following three RIS schemes:

- **RIS-enabled FL system with DP:** In this scheme, Algorithm 1 is applied to solve problem \mathcal{P} .
- **RIS-enabled FL system without DP:** In this scheme, we remove the privacy constraints for the baseline without DP, i.e., only the second term in (32) exists.
- **FL system without RIS:** In this scheme, we set $\Theta_t(i) = \mathbf{0}$ for the baseline without RIS but with DP [34].

The system parameters used in the simulations are summarized in Table II for reference. We also simulate a practical

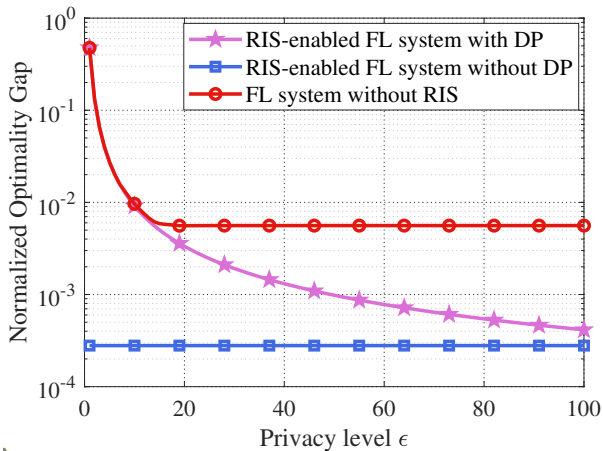


Fig. 5: Learning accuracy of three RIS schemes under different privacy levels.

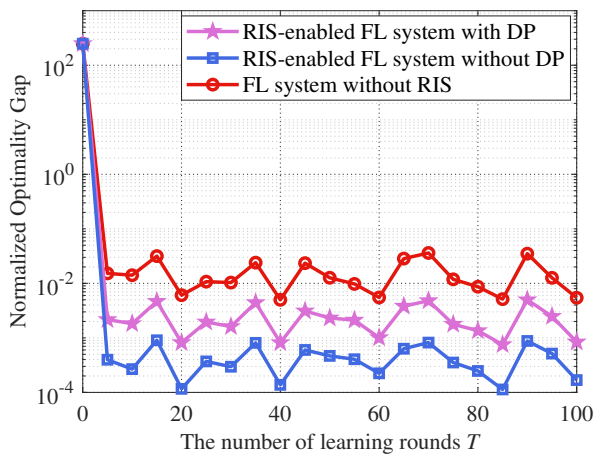


Fig. 7: Learning accuracy of three RIS schemes under different numbers of learning rounds.

Parameter	Value	Parameter	Value	Parameter	Value
K	10	N	30	I	5
D_k	1000	r	0.1	T	30
κ_{IB}	5	κ_{DI}	0	κ_{DB}	5
ϵ	20	δ	0.01	SNR	35

TABLE II: System parameters.

IoT-based affective computing FL scenario [63] with high dimensional and nonconvex settings, which will be presented in Section V-C.

B. Learning Accuracy under Different Conditions

To investigate the improvements of learning accuracy achieved by RIS, we compare the learning accuracy of the three RIS schemes based on the ridge regression model from five aspects: privacy levels ϵ , SNR levels, the number of learning rounds T , the impact of system heterogeneity r , and the number of RIS elements N . We also simulate a high dimensional setting based on the CIFAR-10 dataset and a nonconvex setting based on the MNIST dataset.

We first illustrate the relationship between learning accuracy and privacy level ϵ in Fig. 5. As an extension of Fig. 3, we demonstrate that with the relaxation of privacy level, i.e.,

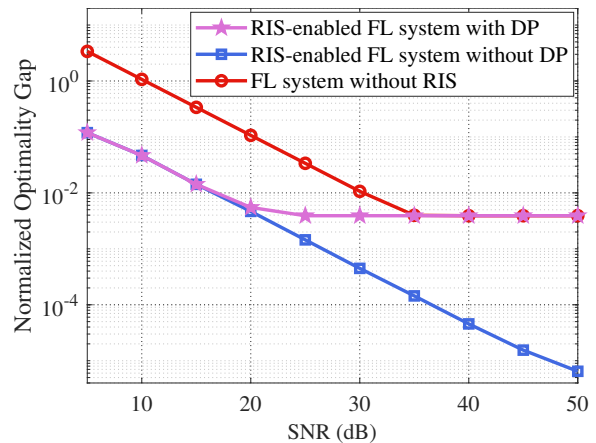


Fig. 6: Learning accuracy of three RIS schemes under various noisy environments.

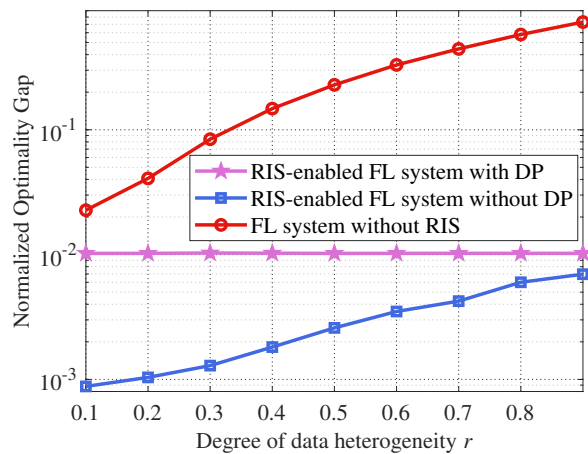


Fig. 8: Learning accuracy of three RIS schemes under various degrees of heterogeneity.

for larger values of ϵ , the RIS-enabled FL system achieves a higher learning performance gain compared to the case without RIS which is restricted by unfavorable wireless channel propagations. Instead, RIS has no impact on the learning performance when the privacy level is strict, i.e., the privacy field presented in **Theorem 3**. Besides, comparing the learning accuracy of the RIS-enabled FL system with DP and the case without DP, we note that the privacy guarantee is achieved at the expense of losing learning accuracy, i.e., higher privacy (smaller value of ϵ) indicates lower learning accuracy.

In Fig. 6, we focus on the learning accuracy of the RIS-enabled FL systems in the noisy wireless environment, i.e., various levels of SNR. It shows that, with the increase of SNR, the DP-restricted schemes achieve the same learning accuracy, i.e., around 4×10^{-3} , under the same privacy and power constraints. Besides, we note that the RIS-enabled FL systems achieve a notable improvement in learning accuracy compared to the FL systems without RIS, especially when SNR is low. This indicates that the RIS-enabled FL systems are more adaptable to noisy wireless channels. Furthermore, Fig. 6 shows that the RIS-enabled FL system with DP achieves close accuracy with the case without DP when SNR < 20. This indicates that privacy guarantee can be ensured freely [34].

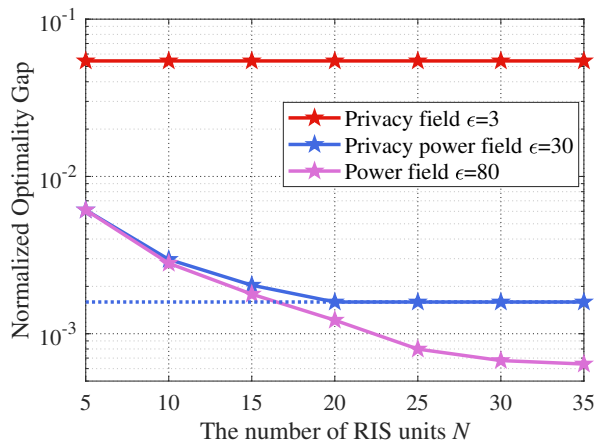


Fig. 9: Learning accuracy of the RIS-enabled FL system with DP under different privacy level ϵ .

The impact brought by the number of learning rounds T or total communication blocks on the learning accuracy is illustrated in Fig. 7, where the oscillation comes from the newly introduced wireless noise in each communication block. We observe that without considering the effect of noise, the number of learning rounds T has no evident effect on the accuracy after running enough number of training rounds for gradient descent due to the adaptive selection of $\{\beta, \tau_r\}$ performed in **Theorem 3**. To make it precise, β can flexibly adjust the selection of $\eta_t(i)$ to ensure that it satisfies all constraints with the increase of T . Moreover, the RIS-enabled FL systems achieve higher accuracy and better robustness to the newly added wireless channel noise.

Fig. 8 shows the learning accuracy of three RIS schemes among various degrees of system heterogeneity r . For simplicity, one edge device is assigned more data points while the rest are evenly distributed to the remaining edge devices [34]. Simulation results show the negative influence brought by the high-heterogeneous system on accuracy. Besides, compared to the FL systems without RIS, the RIS-enabled FL systems are more robust due to the interaction between channel condition and system heterogeneity in (32). Furthermore, Fig. 8 serves as a promising result for the design of anti-heterogeneous FL systems by deploying RIS to weaken heterogeneity.

Fig. 9 illustrates the impacts of the number of reflecting elements N at RIS on the learning accuracy under three fields presented in **Theorem 3**. From Fig. 9, we verify that the learning accuracy cannot be significantly improved when the privacy level is extremely strict (privacy field), while the benefits of deploying RIS emerge when the privacy level is relaxing. Besides, we note that with the increase of N , the reconfigurable capability of RIS enhances, yielding high learning accuracy. However, due to the existence of privacy constraints, this improvement of learning accuracy may slow down when N becomes large.

Fig. 10 and Fig. 11 show the learning accuracy of three RIS schemes on the MNIST and CIFAR-10 datasets, respectively. Specifically, we train a logistic regression model on the CIFAR-10 dataset for high dimensional settings and a neural network on MNIST for nonconvex settings. The neural

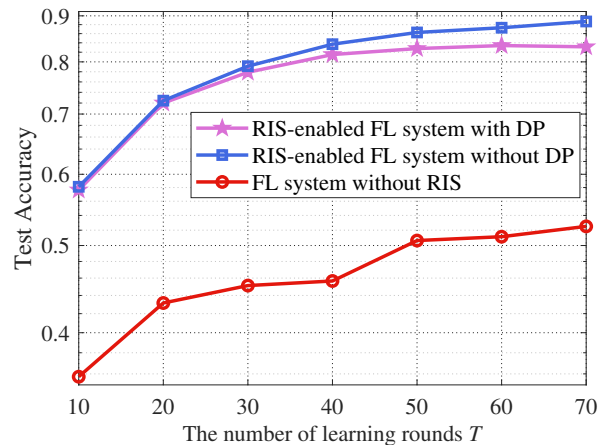


Fig. 10: Test accuracy of the three RIS schemes with MNIST dataset.

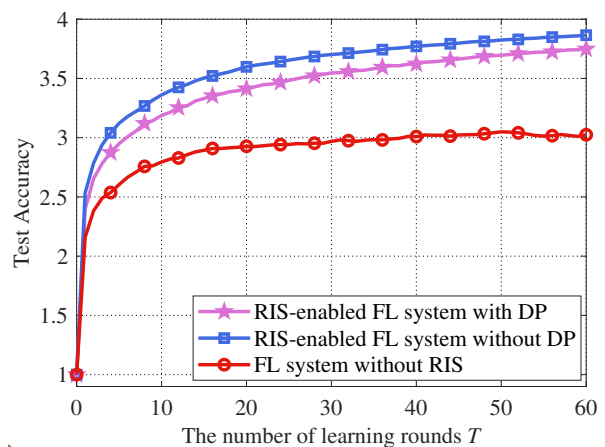


Fig. 11: Relative test accuracy of the three RIS schemes with CIFAR-10 dataset.

network model parameter θ with dimension $d = 79510$ is comprised of the first-layer parameter $\mathbf{W}_1 \in \mathbb{R}^{100 \times 785}$ and the second-layer parameter $\mathbf{W}_2 \in \mathbb{R}^{10 \times 101}$. For high-privacy and noisy environment, we reset the privacy level ϵ to be 10, the SNR level to be 5 dB, the number of communication blocks in one learning round I to be 10, and the Rice factor of \mathbf{q}_{DB} to be 0 (Rayleigh channel). Fig. 10 and Fig. 11 indicate that the RIS-enabled FL system with DP enjoys higher accuracy and better robustness to the wireless channel noise compared to the FL system without RIS. Besides, the accuracy of the RIS-enabled FL system is close to the case without DP. Furthermore, we can observe that our proposed methods can achieve good performance even for nonconvex learning tasks.

C. Differentially Private FL for Wearable IoT-Based Biomedical Monitoring

Driven by the massive amounts of biomedical data generated from widespread IoT edge devices, affective computing has become a field of interest in biomedical informatics [64]. Affective computing is a promising technique that recognizes a person's emotional state based on the physiological signals and images, e.g., photoplethysmogram (PPG) based heart activity, to detect the link between physical health and emotional

	High privacy, Low SNR ($\epsilon = 10$, SNR = 3 dB)	High privacy, High SNR ($\epsilon = 10$, SNR = 10 dB)	Low privacy, Low SNR ($\epsilon = 80$, SNR = 3 dB)	Low privacy, High SNR ($\epsilon = 80$, SNR = 10 dB)
RIS-enabled FL system with DP	0.7308	0.7308	0.7620	0.7716
RIS-enabled FL system without DP	0.7692	0.7716	0.7692	0.7716
FL system without RIS	0.6827	0.7260	0.6851	0.7428

TABLE III: Classification accuracy of various FL systems for stress detection dataset under different privacy and SNR levels.

states. To integrate distributed health data analysis and privacy protection, the authors in [63] established a practical IoT-based wearable biomedical monitoring scenario and provided a first attempt on the application of privacy-preserving FL to IoT-based affective computing. Specifically, 32 public school teachers from Turkey participated in the IoT-based stress detection experiment, where each teacher was required to wear wrist-worn wearable IoT devices and experience three different emotional sessions (baseline, lecture, exam). After each session, the heart activity features collected by wearable IoT devices and the mental state report from each teacher were gathered to construct the stress detection dataset. Besides, the collected data is distributed unevenly across $K = 26$ private edge devices, which are orchestrated by an edge server to collaboratively train a global stress detection model. Inspired by this, we simulate a practical wireless IoT-based stress detection FL scenario with DP guarantees to test the learning performance of three RIS schemes.

We train a neural network on the stress detection dataset whose model parameter θ with dimension $d = 12002$ consists of the the first-layer parameter $\mathbf{W}_1 \in \mathbb{R}^{100 \times 17}$, the second-layer parameter $\mathbf{W}_2 \in \mathbb{R}^{100 \times 101}$ and the third-layer parameter $\mathbf{W}_3 \in \mathbb{R}^{2 \times 101}$. The classification accuracy on the stress detection dataset under different levels of privacy and SNR is presented in Table III. It can be observed that the RIS-enabled FL system with DP is capable of outperforming the FL system without RIS in terms of classification accuracy and robustness to wireless noise. The RIS-enabled system with DP can also achieve similar performance compared with the system without DP.

VI. CONCLUSIONS

In this paper, we developed an RIS-enable differentially private FL system by leveraging the reconfigurability of channel propagation via RIS and the property of waveform superposition via AirComp. We theoretically characterized the convergence behavior of the over-the-air FL algorithm, for which a system optimization problem was established to achieve better learning accuracy under the privacy and transmit power constraints. We further proposed a two-step low-rank optimization framework to minimize the learning optimality gap, by jointly optimizing the power allocation, artificial noise, and reflecting coefficients of RIS during the learning procedure. Through convergence analysis and system optimization, we revealed that the RIS-enabled FL system is able to achieve higher system SNR and boost the receive signal power, thereby improving learning accuracy performance while satisfying the privacy requirements. Numerical results also demonstrated that the proposed FL system can achieve higher learning accuracy and privacy than the benchmarks.

APPENDIX A PROOF OF THEOREM 1

For each edge device k , we note that the local gradient $\mathbf{g}_{k,t}$ is divided into I e -dimensional sub-signals. Based on (14), we arrive at the equivalent channel noise vector

$$\hat{\mathbf{w}}_t = \left[\frac{\mathbf{w}_t^T(1)}{\sqrt{\eta_t(1)}}, \dots, \frac{\mathbf{w}_t^T(I)}{\sqrt{\eta_t(I)}} \right]^T. \quad (43)$$

Then the estimated $\hat{\mathbf{g}}_t$ at the edge server can be expressed as

$$\hat{\mathbf{g}}_t = \mathbf{g}_t + \frac{1}{KD} \sum_{k=1}^K \text{Re}\{\mathbf{n}_{k,t}\} + \frac{1}{KD} \text{Re}\{\hat{\mathbf{w}}_t\}. \quad (44)$$

Hence, under Assumption 2, we have the following inequality

$$\begin{aligned} F(\theta_{t+1}) &\leq F(\theta_t) - \lambda \mathbf{g}_t^T \hat{\mathbf{g}}_t + \frac{L\lambda^2}{2} \|\hat{\mathbf{g}}_t\|^2 \\ &= F(\theta_t) - \lambda \|\mathbf{g}_t\|^2 - \frac{\lambda}{KD} \sum_{k=1}^K \text{Re}\{\mathbf{g}_t^T \mathbf{n}_{k,t}\} - \frac{\lambda \text{Re}\{\mathbf{g}_t^T \hat{\mathbf{w}}_t\}}{KD} \\ &\quad + \frac{L\lambda^2}{2} \left\| \mathbf{g}_t + \frac{1}{KD} \sum_{k=1}^K \text{Re}\{\mathbf{n}_{k,t}\} + \frac{1}{KD} \text{Re}\{\hat{\mathbf{w}}_t\} \right\|^2. \end{aligned}$$

Recalling that $\mathbf{n}_{k,t} = [\mathbf{n}_{k,t}^T(1), \dots, \mathbf{n}_{k,t}^T(I)]^T$ with $\mathbf{n}_{k,t}(i) \sim \mathcal{CN}(\mathbf{0}, \sigma_{k,t}^2(i) \mathbf{I}_e)$ and given $\lambda = 1/L$, by taking the expectations over the additive noise (including the artificial and wireless channel noise) on both sides of the above inequality, we obtain

$$\begin{aligned} \mathbb{E}[F(\theta_{t+1})] &\leq F(\theta_t) + \left(\frac{L}{2} \lambda^2 - \lambda \right) \|\mathbf{g}_t\|^2 + \frac{L\lambda^2}{2} \times \\ &\quad \frac{1}{(KD)^2} \mathbb{E} \left[\left\| \sum_{k=1}^K \text{Re}\{[\mathbf{n}_{k,t}^T(1), \dots, \mathbf{n}_{k,t}^T(I)]^T\} + \text{Re}\{\hat{\mathbf{w}}_t\} \right\|^2 \right] \\ &\leq F(\theta_t) - \frac{1}{2L} \|\mathbf{g}_t\|^2 + \frac{e}{4L(KD)^2} \left(\sum_{k=1}^K \sum_{i=1}^I \sigma_{k,t}^2(i) + \sum_{i=1}^I \frac{N_0}{\eta_t(i)} \right). \end{aligned}$$

According to (16), by setting $\theta = \theta^*$ and $\theta' = \theta_t$, we have

$$\frac{1}{2} \|\nabla F(\theta_t)\|^2 \geq \mu [F(\theta_t) - F^*]. \quad (45)$$

Therefore, subtracting the optimal value F^* at both sides yields

$$\begin{aligned} \mathbb{E}[F(\theta_{t+1})] - F^* &\leq \left(1 - \frac{\mu}{L}\right) [F(\theta_t) - F^*] + \\ &\quad \frac{e}{4L(KD)^2} \left(\sum_{k=1}^K \sum_{i=1}^I \sigma_{k,t}^2(i) + \sum_{i=1}^I \frac{N_0}{\eta_t(i)} \right). \end{aligned} \quad (46)$$

Finally, the expected result is obtained by applying (46) iteratively through T learning rounds. \square

APPENDIX B
PROOF OF THEOREM 2

The proving process is based on the advanced literature [30], [34], [40]. We focus on the privacy constraint of the k -th edge device based on the aggregated signals $\mathbf{r} = \{\mathbf{r}_t\}_{t=1}^T$ at the edge server. It is worth noting that, without traditional lightweight assumption, our transmission model faces a more practical scenario where one learning round consists of I communication blocks.

According to (8), the privacy loss after T learning rounds can be expressed as

$$\begin{aligned} \mathcal{L}_{\mathcal{D}_k, \mathcal{D}'_k}(\mathbf{r}) &= \ln \left\{ \prod_{t=1}^T \frac{\Pr[\mathbf{r}_t | \mathbf{r}_{t-1}, \dots, \mathbf{r}_1; \mathcal{D}_k]}{\Pr[\mathbf{r}_t | \mathbf{r}_{t-1}, \dots, \mathbf{r}_1; \mathcal{D}'_k]} \right\} \\ &= \sum_{t=1}^T \ln \left\{ \frac{\Pr[\mathbf{r}_t | \mathbf{r}_{t-1}, \dots, \mathbf{r}_1; \mathcal{D}_k]}{\Pr[\mathbf{r}_t | \mathbf{r}_{t-1}, \dots, \mathbf{r}_1; \mathcal{D}'_k]} \right\}. \end{aligned} \quad (47)$$

The effective noise \mathbf{q}_t in (20) is a complex Gaussian random vector with statistically independent elements. Besides, recalling that the noise vector $\mathbf{w}_t(i) \sim \mathcal{CN}(\mathbf{0}, N_0 \mathbf{I}_e)$ and $\mathbf{n}_{k,t}(i) \sim \mathcal{CN}(\mathbf{0}, \sigma_{k,t}^2(i) \mathbf{I}_e)$, we obtain the pseudo-covariance matrix of \mathbf{q}_t , which is given by

$$\mathbf{J}_t = \mathbb{E}[\mathbf{q}_t (\mathbf{q}_t)^T] = \mathbf{0}, \quad (48)$$

and the covariance matrix of \mathbf{q}_t can be expressed as

$$\mathbf{\Sigma}_t = \mathbb{E}[\mathbf{q}_t (\mathbf{q}_t)^H] = \begin{bmatrix} \Lambda_t(1) & \cdots & \mathbf{0} \\ \vdots & \ddots & \vdots \\ \mathbf{0} & \cdots & \Lambda_t(I) \end{bmatrix}, \quad (49)$$

where

$$\Lambda_t(i) = \left(\eta_t(i) \sum_{k=1}^K \sigma_{k,t}^2(i) + N_0 \right) \mathbf{I}_e, \quad \forall i \in [I] \quad (50)$$

denotes the diagonal positive semi-definite covariance matrix of $\mathbf{q}_t(i)$, which indicates that $\mathbf{\Sigma}_t$ is a diagonal positive semi-definite matrix.

According to [65, Appendix. A], it is easy to verify that \mathbf{q}_t is a complex random vector with circular symmetry property, whose probability density function (pdf) is given by

$$p(\mathbf{q}_t) = \frac{1}{\pi^d \det(\mathbf{\Sigma}_t)} \exp\left(-\mathbf{q}_t^H \mathbf{\Sigma}_t^{-1} \mathbf{q}_t\right). \quad (51)$$

Therefore, for the analysis of sensitivity, we further denote the effective noise based on dataset \mathcal{D}_k as $\mathbf{z}_{k,t} = [\mathbf{z}_{k,t}^T(1), \dots, \mathbf{z}_{k,t}^T(I)]^T$ with

$$\mathbf{z}_{k,t}(i) = \mathbf{r}_t(i) - \sqrt{\eta_t(i)} D_k \mathbf{g}_{k,t}(i; \mathcal{D}_k) - \nu_{k,t}(i),$$

where $\nu_{k,t}(i)$ denotes the second constant term in (19) and $\mathbf{g}_{k,t}(i; \mathcal{D}_k)$ represents the updated gradient based on \mathcal{D}_k , thus we can obtain

$$\Pr[\mathbf{r}_t | \mathbf{r}_{t-1}, \dots, \mathbf{r}_1; \mathcal{D}_k] = \frac{1}{\pi^d \det(\mathbf{\Sigma}_t)} \exp\left(-\mathbf{z}_{k,t}^H \mathbf{\Sigma}_t^{-1} \mathbf{z}_{k,t}\right).$$

Furthermore, according to (22), $\mathbf{z}_{k,t} + \mathbf{u}_{k,t}$ represents the effective noise based on dataset \mathcal{D}'_k . Hence, substituting them

into (47), we have

$$\begin{aligned} \mathcal{L}_{\mathcal{D}_k, \mathcal{D}'_k}(\mathbf{r}) &= \sum_{t=1}^T \left[(\mathbf{z}_{k,t} + \mathbf{u}_{k,t})^H \mathbf{\Sigma}_t^{-1} (\mathbf{z}_{k,t} + \mathbf{u}_{k,t}) - (\mathbf{z}_{k,t})^H \mathbf{\Sigma}_t^{-1} \mathbf{z}_{k,t} \right] \\ &= \sum_{t=1}^T [2\text{Re}\{\mathbf{u}_{k,t}^H \mathbf{\Sigma}_t^{-1} \mathbf{z}_{k,t}\} + \mathbf{u}_{k,t}^H \mathbf{\Sigma}_t^{-1} \mathbf{u}_{k,t}]. \end{aligned}$$

Based on (9), given the DP parameter pair (ϵ, δ) , the privacy violation probability bound can be expressed as

$$\begin{aligned} \Pr\left(\left|\mathcal{L}_{\mathcal{D}_k, \mathcal{D}'_k}(\mathbf{r})\right| > \epsilon\right) &\stackrel{(a)}{\leq} \Pr\left[\left|\text{Re}\{\mathbf{u}_{k,t}^H \mathbf{\Sigma}_t^{-1} \mathbf{z}_{k,t}\}\right| > \frac{\epsilon}{2} - \frac{1}{2} \sum_{t=1}^T \mathbf{u}_{k,t}^H \mathbf{\Sigma}_t^{-1} \mathbf{u}_{k,t}\right] \\ &= 2 \Pr\left[\sum_{t=1}^T \text{Re}\{\mathbf{u}_{k,t}^H \mathbf{\Sigma}_t^{-1} \mathbf{z}_{k,t}\} > \frac{\epsilon}{2} - \frac{1}{2} \sum_{t=1}^T \mathbf{u}_{k,t}^H \mathbf{\Sigma}_t^{-1} \mathbf{u}_{k,t}\right] \\ &\triangleq 2 \Pr(Y_k > c_k), \end{aligned}$$

where (a) comes from the inequality $\Pr(|X + e| > \epsilon) \leq \Pr(|X| > \epsilon - e)$ for $e \geq 0$. We note that $\mathbf{z}_{k,t} \sim \mathcal{CN}(\mathbf{0}, \mathbf{\Sigma}_t)$ and $\mathbf{\Sigma}_t$ is a diagonal matrix. Hence, it is easy to verify that $\mathbf{\Sigma}_t^{-1/2} \mathbf{z}_{k,t} \sim \mathcal{CN}(\mathbf{0}, \mathbf{I}_d)$, which leads to $\mathbf{u}_{k,t}^H \mathbf{\Sigma}_t^{-1} \mathbf{z}_{k,t} \sim \mathcal{CN}(\mathbf{0}, \mathbf{u}_{k,t}^H \mathbf{\Sigma}_t^{-1} \mathbf{u}_{k,t})$. As a result, considering the fact that any $\mathbf{z}_{k,t}$ is statistical independent of each other, Y_k is a random variable according to $\mathcal{N}(0, \frac{1}{2} \sum_{t=1}^T \mathbf{u}_{k,t}^H \mathbf{\Sigma}_t^{-1} \mathbf{u}_{k,t})$.

According to (24) and by denoting

$$\xi_t \leq \eta_t(i) \sum_{k=1}^K \sigma_{k,t}^2(i) + N_0, \quad \forall i, t$$

as a lower bound of the power of effective noise, we have the following inequalities

$$v_k^2 \triangleq \sum_{t=1}^T \frac{2\gamma_t^2}{\xi_t} \max_{i \in [I]} \{\eta_t(i)\} \stackrel{(a)}{\geq} \sum_{t=1}^T \frac{\|\mathbf{u}_{k,t}\|^2}{2\xi_t} \stackrel{(b)}{\geq} \frac{1}{2} \sum_{t=1}^T \mathbf{u}_{k,t}^H \mathbf{\Sigma}_t^{-1} \mathbf{u}_{k,t},$$

$$\hat{c}_k \leq \frac{\epsilon}{2} - \sum_{t=1}^T \frac{2\gamma_t^2}{\xi_t} \max_{i \in [I]} \{\eta_t(i)\} \stackrel{(c)}{\leq} \frac{\epsilon}{2} - \sum_{t=1}^T \frac{\|\mathbf{u}_{k,t}\|^2}{2\xi_t} \leq c_k,$$

where (a) and (c) comes from the upper bound in (24), and (b) is obtained by (49). Based on this, we introduce another random variable Ξ_k according to $\mathcal{CN}(0, v_k^2)$. Thus, we arrive at the following inequalities:

$$\Pr(Y_k > c_k) \leq \Pr(\Xi_k > c_k) \leq \Pr(\Xi_k > \hat{c}_k). \quad (52)$$

Finally, according to Mill's inequality, we can obtain

$$\Pr(|Y_k| > c_k) < \sqrt{\frac{2}{\pi}} \frac{v_k}{\hat{c}_k} \exp\left(-\frac{\hat{c}_k^2}{2v_k^2}\right) < \delta,$$

followed by solving an equation based on the monotonicity property of function $C(x) = \sqrt{\pi} x e^{x^2}$, then we arrive at the expected result in (25). \square

APPENDIX C
PROOF OF THEOREM 3

To start, by using the change of variables, we define the following new relationships:

$$a_{k,t}^i = \sigma_{k,t}^2(i), \quad b_t^i = \eta_t^{-1}(i), \quad c_t^i = \xi_t b_t^i = \xi_t \eta_t^{-1}(i). \quad (53)$$

Thus, it is easy to verify that $a_{k,t}^i \geq 0$ and $b_t^i, c_t^i > 0$. Besides, we also denote

$$d_t = \frac{\xi_t}{\max_i \{\eta_t(i)\}} = \xi_t \min_i \{b_t^i\}, \quad \forall t, \quad (54)$$

which yields an inherent constraint $d_t \leq c_t^i, \forall i, t$.

For short, we omit the superscript and subscript when describing the optimization variables, e.g., $a_{k,t}^i$ as a . Therefore, problem \mathcal{P}_1 can be transformed into problem $\mathcal{P}_{1.1}$:

$$\min_{\{a,b,c,d\}} \sum_{t=1}^T \left(1 - \frac{\mu}{L}\right)^{-t} \left(\sum_{k=1}^K \sum_{i=1}^I a_{k,t}^i + N_0 \sum_{i=1}^I b_t^i \right) \quad (55a)$$

$$\text{subject to} \quad \sum_{t=1}^T \frac{4\gamma_t^2}{d_t} - \mathcal{R}_{dp} \leq 0, \quad (55b)$$

$$c_t^i - \sum_{k=1}^K a_{k,t}^i - N_0 b_t^i \leq 0, \quad \forall i, t, \quad (55c)$$

$$D^2 \zeta_{k,t}^2(i) + e a_{k,t}^i \leq P_0 |h_{k,t}(i)|^2 b_t^i, \quad \forall i, k, t, \quad (55d)$$

$$d_t - c_t^i \leq 0, \quad \forall i, t, \quad (55e)$$

$$a_{k,t}^i \geq 0, \quad b_t^i \geq 0, \quad c_t^i \geq 0, \quad d_t \geq 0, \quad \forall i, k, t, \quad (55f)$$

which is a pure convex problem and can be tackled by KKT conditions. Above all, the Lagrange function is given as

$$\begin{aligned} \mathcal{L} = & \sum_{t=1}^T \left(1 - \frac{\mu}{L}\right)^{-t} \left(\sum_{k=1}^K \sum_{i=1}^I a_{k,t}^i + N_0 \sum_{i=1}^I b_t^i \right) \\ & + \beta \left(\sum_{t=1}^T \frac{4\gamma_t^2}{d_t} - \mathcal{R}_{dp} \right) - \sum_{t=1}^T \sum_{k=1}^K \sum_{i=1}^I \varphi_{k,t}^i a_{k,t}^i \\ & + \sum_{t=1}^T \sum_{i=1}^I \iota_t^i \left(c_t^i - \sum_{k=1}^K a_{k,t}^i - N_0 b_t^i \right) + \sum_{t=1}^T \sum_{i=1}^I u_t^i (d_t - c_t^i) \\ & + \sum_{t=1}^T \sum_{k=1}^K \sum_{i=1}^I \psi_{k,t}^i \left(D^2 \zeta_{k,t}^2(i) + e a_{k,t}^i - P_0 |h_{k,t}(i)|^2 b_t^i \right), \end{aligned}$$

where $\beta, \iota_t^i, u_t^i, \psi_{k,t}^i, \varphi_{k,t}^i \geq 0$ represent the Lagrange multipliers and for simplicity, we omit some obviously zero terms. We denote variables with " \sim " as the optimal solutions satisfying KKT conditions, e.g., $\tilde{a}_{k,t}^i$ denotes the optimal $a_{k,t}^i$. Hence, we can obtain the following relationships:

$$\frac{\partial \mathcal{L}}{\partial a_{k,t}^i} = \left(1 - \frac{\mu}{L}\right)^{-t} - \iota_t^i + e \psi_{k,t}^i - \varphi_{k,t}^i = 0, \quad (56a)$$

$$\frac{\partial \mathcal{L}}{\partial b_t^i} = N_0 \left(1 - \frac{\mu}{L}\right)^{-t} - N_0 \iota_t^i - P_0 \sum_{k=1}^K \psi_{k,t}^i |h_{k,t}(i)|^2 = 0, \quad (56b)$$

$$\frac{\partial \mathcal{L}}{\partial c_t^i} = \iota_t^i - u_t^i = 0, \quad (56c)$$

$$\frac{\partial \mathcal{L}}{\partial d_t} = -\beta \frac{4\gamma_t^2}{d_t^2} + \sum_{i=1}^I u_t^i = 0, \quad (56d)$$

which indicate that at least one of $\tilde{\iota}_t^i$ and $\tilde{\varphi}_{k,t}^i$ is greater than 0. Based on this, we mainly focus on the following three conditions and elaborate their optimality.

Power field: On the one hand, we first focus on a simple case where the inequality in (55b) strictly holds, i.e., the privacy constraint is not dominant. Hence, according to complementary slackness condition, we immediately get

$$\tilde{\beta} = \tilde{u}_t^i = \tilde{\iota}_t^i = 0, \quad \forall i, t. \quad (57)$$

Furthermore, we have $\tilde{\varphi}_{k,t}^i > 0$ based on (56a) which also implies $\tilde{a}_{k,t}^i = 0$. Hence, the power constraint (55d) becomes the unique one that restricts the learning accuracy. Based on this, we arrive at the unique optimal solution in this case, i.e.,

$$\tilde{b}_t^i = \frac{1}{P_0} \max_{k \in [K]} \frac{D^2 \zeta_{k,t}^2(i)}{|h_{k,t}(i)|^2}. \quad (58)$$

On the other hand, we turn to the difficult multi-solution case where the privacy constraint (55b) is stringent with $\tilde{\beta} \neq 0$, which results in the following equality:

$$\sum_{t=1}^T \frac{4\gamma_t^2}{d_t} - \mathcal{R}_{dp} = 0. \quad (59)$$

Motivated by the previous condition, we set $\tilde{a}_{k,t}^i = 0$, which saves the communication and power resources of the edge server. Hence, we arrive at the following two conditions.

Privacy field: We first focus on the case where only the privacy constraint takes effect, which indicates (55d) strictly holds, i.e.,

$$\tilde{b}_t > \frac{1}{P_0} \max_{i,k} \frac{D^2 \zeta_{k,t}^2(i)}{|h_{k,t}(i)|^2}, \quad (60)$$

yielding $\tilde{\psi}_{k,t}^i = 0$. Hence, based on (56b) and (56c), we obtain

$$\tilde{u}_t^i = \tilde{\iota}_t^i = \left(1 - \frac{\mu}{L}\right)^{-t}, \quad \forall i, t. \quad (61)$$

Besides, combining (56d) and complementary slackness condition, we further get

$$\tilde{d}_t = \tilde{c}_t^i = N_0 \tilde{b}_t^i = \frac{2\gamma_t}{\sqrt{I}} (\tilde{\beta})^{\frac{1}{2}} \left(1 - \frac{\mu}{L}\right)^{\frac{1}{2}}, \quad (62)$$

which indicates \tilde{b}_t^i remains constant during one learning round, and for short, we denote $\tilde{b}_t = \tilde{b}_t^i, \forall i$. In summary, the optimal conditions of \tilde{b}_t are given by (59), (60), and (62).

Privacy-power field: Now, we turn to analyze the case where the dual constraints of privacy and power take effect, i.e., there exist some $\tilde{c}_t^i \neq \tilde{d}_t$ which lead to $\tilde{u}_t^i = \tilde{\iota}_t^i = 0$. Besides, from (56b), we can verify that there exist $\tilde{\psi}_{k,t}^i \neq 0$ based on the power constraints of all edge devices. Remarkably, \tilde{b}_t^i remains constant across all edge devices in the i -th communication block of learning round t , so it must meet all power constraints and strictly satisfy a certain one, i.e.,

$$\tilde{b}_t^i = \frac{1}{P_0} \max_k \frac{D^2 \zeta_{k,t}^2(i)}{|h_{k,t}(i)|^2}. \quad (63)$$

As for the other $\tilde{u}_t^i \neq 0$, we consider it as a generalized

version of (61), i.e., some communication blocks are restricted by privacy while the others are power. For analytical ease, we introduce parameter τ_t to represent the number of communication blocks limited by privacy in the t -th learning round, i.e., $\tilde{u}_{k,t}^i \neq 0$. Hence, (56d) can be reformulated as

$$\tau_t \left(1 - \frac{\mu}{L}\right)^{-t} = \frac{4\gamma_t^2}{d_t^2} \tilde{\beta}. \quad (64)$$

For instance, if all communication blocks are restricted by privacy, τ_t is set to I which is the same as (62), i.e., **Privacy field**. Therefore, considering the above two cases, we arrive at the expected result by elaborately selecting τ_t in each learning round t and parameter $\tilde{\beta}$ to strictly meet (59).

Finally, according to (53), we obtain the expected result. \square

REFERENCES

- [1] K. B. Letaief, W. Chen, Y. Shi, J. Zhang, and Y.-J. A. Zhang, "The roadmap to 6G: AI empowered wireless networks," *IEEE Commun. Mag.*, vol. 57, no. 8, pp. 84–90, 2019.
- [2] B. McMahan, E. Moore, D. Ramage, S. Hampson, and B. A. Y. Arcas, "Communication-efficient learning of deep networks from decentralized data," in *Proc. Int. Conf. Artif. Intell. Stat. (AISTATS)*, vol. 54, pp. 1273–1282, PMLR, 2017.
- [3] K. B. Letaief, Y. Shi, J. Lu, and J. Lu, "Edge artificial intelligence for 6G: Vision, enabling technologies, and applications," *IEEE J. Sel. Areas Commun.*, vol. 40, no. 1, pp. 5–36, 2022.
- [4] Y. Shi, K. Yang, T. Jiang, J. Zhang, and K. B. Letaief, "Communication-efficient edge AI: Algorithms and systems," *IEEE Commun. Surveys Tuts.*, vol. 22, no. 4, pp. 2167–2191, 2020.
- [5] D. C. Nguyen, M. Ding, P. N. Pathirana, A. Seneviratne, J. Li, and H. Vincent Poor, "Federated learning for internet of things: A comprehensive survey," *IEEE Commun. Surveys Tuts.*, vol. 23, no. 3, pp. 1622–1658, 2021.
- [6] A. Imteaj, U. Thakker, S. Wang, J. Li, and M. H. Amini, "A survey on federated learning for resource-constrained IoT devices," *IEEE Internet of Things J.*, 2021, Doi: 10.1109/JIOT.2021.3095077.
- [7] J. Wang, Z. Charles, Z. Xu, G. Joshi, H. B. McMahan, M. Al-Shedivat, G. Andrew, S. Avestimehr, K. Daly, D. Data, et al., "A field guide to federated optimization," *arXiv:2107.06917*. [Online]. <https://arxiv.org/pdf/2107.06917.pdf>, 2021.
- [8] N. Rieke, J. Hancox, W. Li, F. Milletari, H. R. Roth, S. Albarqouni, S. Bakas, M. N. Galtier, B. A. Landman, K. Maier-Hein, et al., "The future of digital health with federated learning," *NPJ digital medicine*, vol. 3, no. 1, pp. 1–7, 2020.
- [9] H. Jin, X. Dai, J. Xiao, B. Li, H. Li, and Y. Zhang, "Cross-cluster federated learning and blockchain for internet of medical things," *IEEE Internet Things J.*, 2021.
- [10] V. Hayyolalam, M. Aloqaily, O. Ozkasap, and M. Guizani, "Edge intelligence for empowering iot-based healthcare systems," *IEEE Wireless Communications*, vol. 28, no. 3, pp. 6–14, 2021.
- [11] Z. Yan, J. Wicaksana, Z. Wang, X. Yang, and K.-T. Cheng, "Variation-aware federated learning with multi-source decentralized medical image data," *IEEE J. Biomed. Health Inform.*, vol. 25, no. 7, pp. 2615–2628, 2021.
- [12] S. Chen, D. Xue, G. Chuai, Q. Yang, and Q. Liu, "FI-QSAR: a federated learning-based qsar prototype for collaborative drug discovery," *Bioinformatics*, vol. 36, no. 22–23, pp. 5492–5498, 2020.
- [13] S. Warnat-Herresthal, H. Schultze, K. L. Shastri, S. Manamohan, S. Mukherjee, V. Garg, R. Sarveswara, K. Händler, P. Pickkers, N. A. Aziz, et al., "Swarm learning for decentralized and confidential clinical machine learning," *Nature*, vol. 594, no. 7862, pp. 265–270, 2021.
- [14] T. Li, A. K. Sahu, A. Talwalkar, and V. Smith, "Federated learning: Challenges, methods, and future directions," *IEEE Signal Process. Mag.*, vol. 37, no. 3, pp. 50–60, 2020.
- [15] U. Sennur, A. Salman, G. Michael, J. Syed, T. Ravi, and T. Chao, "Private retrieval, computing and learning: Recent progress and future challenges," *arXiv:2108.00026*. [Online]. <https://arxiv.org/pdf/2108.00026.pdf>, 2021.
- [16] K. Yang, T. Jiang, Y. Shi, and Z. Ding, "Federated learning via over-the-air computation," *IEEE Trans. Wireless Commun.*, vol. 19, no. 3, pp. 2022–2035, 2020.
- [17] G. Zhu, Y. Wang, and K. Huang, "Broadband analog aggregation for low-latency federated edge learning," *IEEE Trans. Wireless Commun.*, vol. 19, no. 1, pp. 491–506, 2019.
- [18] M. M. Amiri and D. Gündüz, "Machine learning at the wireless edge: Distributed stochastic gradient descent over-the-air," *IEEE Trans. Signal Process.*, vol. 68, pp. 2155–2169, 2020.
- [19] N. Zhang and M. Tao, "Gradient statistics aware power control for over-the-air federated learning," *IEEE Trans. Wireless Commun.*, vol. 20, no. 8, pp. 5115–5128, 2021.
- [20] K. Yang, Y. Shi, Y. Zhou, Z. Yang, L. Fu, and W. Chen, "Federated machine learning for intelligent IoT via reconfigurable intelligent surface," *IEEE Network*, vol. 34, no. 5, pp. 16–22, 2020.
- [21] Z. Wang, J. Qiu, Y. Zhou, Y. Shi, L. Fu, W. Chen, and K. B. Letaief, "Federated learning via intelligent reflecting surface," *IEEE Trans. Wireless Commun.*, 2021.
- [22] H. Liu, X. Yuan, and Y.-J. A. Zhang, "Reconfigurable intelligent surface enabled federated learning: A unified communication-learning design approach," *IEEE Trans. Wireless Commun.*, 2021, doi:10.1109/TWC.2021.3086116.
- [23] X. Yuan, Y.-J. A. Zhang, Y. Shi, W. Yan, and H. Liu, "Reconfigurable-intelligent-surface empowered wireless communications: Challenges and opportunities," *IEEE Wireless Commun.*, vol. 28, no. 2, pp. 136–143, 2021.
- [24] Q. Wu and R. Zhang, "Intelligent reflecting surface enhanced wireless network via joint active and passive beamforming," *IEEE Trans. Wireless Commun.*, vol. 18, no. 11, pp. 5394–5409, 2019.
- [25] C. Huang, A. Zappone, G. C. Alexandropoulos, M. Debbah, and C. Yuen, "Reconfigurable intelligent surfaces for energy efficiency in wireless communication," *IEEE Trans. Wireless Commun.*, vol. 18, no. 8, pp. 4157–4170, 2019.
- [26] M. Di Renzo, A. Zappone, M. Debbah, M.-S. Alouini, C. Yuen, J. De Rosny, and S. Tretyakov, "Smart radio environments empowered by reconfigurable intelligent surfaces: How it works, state of research, and the road ahead," *IEEE J. Sel. Areas Commun.*, vol. 38, no. 11, pp. 2450–2525, 2020.
- [27] B. Hitaj, G. Ateniese, and F. Perez-Cruz, "Deep models under the GAN: information leakage from collaborative deep learning," in *Proc. of the 2017 ACM SIGSAC Conf. Comput. Commun. Secur.*, pp. 603–618, 2017.
- [28] L. Zhu and S. Han, "Deep leakage from gradients," in *Federated Learning*, pp. 17–31, Springer, 2020.
- [29] J. Geiping, H. Bauermeister, H. Dröge, and M. Moeller, "Inverting gradients—how easy is it to break privacy in federated learning?," *arXiv:2003.14053*. [Online]. <https://arxiv.org/pdf/2003.14053.pdf>, 2020.
- [30] C. Dwork, A. Roth, et al., "The algorithmic foundations of differential privacy," *Found. Trends Theor. Comput. Sci.*, vol. 9, no. 3–4, pp. 211–407, 2014.
- [31] A. M. Girgis, D. Data, S. Diggavi, P. Kairouz, and A. T. Suresh, "Shuffled model of federated learning: Privacy, communication and accuracy trade-offs," *IEEE J. Sel. Areas Commun. Inf. Theory (JSAIT)*, vol. 2, no. 1, pp. 464–478, 2021.
- [32] N. Wu, F. Farokhi, D. Smith, and M. A. Kaafar, "The value of collaboration in convex machine learning with differential privacy," in *2020 IEEE Secur. Priv. (SSP)*, pp. 304–317, IEEE, 2020.
- [33] N. Agarwal, A. T. Suresh, F. Yu, S. Kumar, and H. B. McMahan, "cpSGD: Communication-efficient and differentially-private distributed SGD," *Adv. Neural Inf. Process. Syst.*, pp. 7564–7575, 2018.
- [34] D. Liu and O. Simeone, "Privacy for free: Wireless federated learning via uncoded transmission with adaptive power control," *IEEE J. Sel. Areas Commun.*, vol. 39, no. 1, pp. 170–185, 2020.
- [35] B. Hasircioğlu and D. Gündüz, "Private wireless federated learning with anonymous over-the-air computation," in *2021 IEEE Int. Conf. Acoust. Speech Signal Process. (ICASSP)*, pp. 5195–5199, IEEE, 2021.
- [36] M. Seif, R. Tandon, and M. Li, "Wireless federated learning with local differential privacy," in *2020 IEEE Int. Symp. on Inf. Theory (ISIT)*, pp. 2604–2609, IEEE, 2020.
- [37] Y. Koda, K. Yamamoto, T. Nishio, and M. Morikura, "Differentially private aircomp federated learning with power adaptation harnessing receiver noise," in *GLOBECOM 2020-2020 IEEE Glob. Commun. Conf.*, pp. 1–6, IEEE, 2020.
- [38] M. S. E. Mohamed, W.-T. Chang, and R. Tandon, "Privacy amplification for federated learning via user sampling and wireless aggregation," *IEEE J. Sel. Areas Commun.*, vol. 39, no. 12, pp. 3821–3835, 2021.
- [39] L. Li, L. Yang, X. Guo, Y. Shi, H. Wang, W. Chen, and K. B. Letaief, "Delay analysis of wireless federated learning based on saddle point approximation and large deviation theory," *arXiv:2103.16994*. [Online]. <https://arxiv.org/pdf/2103.16994.pdf>, 2021.

- [40] S. Rezaei Aghdam, E. Amid, M. Furdek, *et al.*, “Privacy-preserving wireless federated learning exploiting inherent hardware impairments,” *arXiv:2102.10639*. [Online]. <https://arxiv.org/pdf/2102.10639.pdf>, 2021.
- [41] T. Sery and K. Cohen, “On analog gradient descent learning over multiple access fading channels,” *IEEE Trans. Signal Process.*, vol. 68, pp. 2897–2911, 2020.
- [42] X. Li, K. Huang, W. Yang, S. Wang, and Z. Zhang, “On the convergence of FedAvg on non-iid data,” *Proc. Int. Conf. Learn. Represent. (ICLR)*, 2020.
- [43] M. M. Amiri and D. Gündüz, “Machine learning at the wireless edge: Distributed stochastic gradient descent over-the-air,” *IEEE Trans. on Signal Process.*, vol. 68, pp. 2155–2169, 2020.
- [44] X. Yu, D. Xu, Y. Sun, D. W. K. Ng, and R. Schober, “Robust and secure wireless communications via intelligent reflecting surfaces,” *IEEE J. Sel. Areas Commun.*, vol. 38, no. 11, pp. 2637–2652, 2020.
- [45] E. Bagdasaryan, O. Poursaeed, and V. Shmatikov, “Differential privacy has disparate impact on model accuracy,” *Adv. Neural Inf. Process. Syst.*, vol. 32, pp. 15479–15488, 2019.
- [46] L. Chen, X. Qin, and G. Wei, “A uniform-forcing transceiver design for over-the-air function computation,” *IEEE Wireless Commun. Lett.*, vol. 7, no. 6, pp. 942–945, 2018.
- [47] E. Dahlman, S. Parkvall, and J. Skold, *4G: LTE/LTE-advanced for mobile broadband*. Academic press, 2013.
- [48] A. Ghosh, J. Zhang, J. G. Andrews, and R. Muhamed, *Fundamentals of LTE*. Pearson Education, 2010.
- [49] M. P. Friedlander and M. Schmidt, “Hybrid deterministic-stochastic methods for data fitting,” *SIAM J. Sci. Comput.*, vol. 34, no. 3, pp. A1380–A1405, 2012.
- [50] A. M.-C. So, J. Zhang, and Y. Ye, “On approximating complex quadratic optimization problems via semidefinite programming relaxations,” *Math. Program.*, vol. 110, no. 1, pp. 93–110, 2007.
- [51] Z.-Q. Luo, W.-K. Ma, A. M.-C. So, Y. Ye, and S. Zhang, “Semidefinite relaxation of quadratic optimization problems,” *IEEE Signal Process. Mag.*, vol. 27, no. 3, pp. 20–34, 2010.
- [52] M. Grant and S. Boyd, “CVX: Matlab software for disciplined convex programming, version 2.1.” <http://cvxr.com/cvx>, Mar. 2014.
- [53] D. Wang and J. Xu, “Differentially private empirical risk minimization with smooth non-convex loss functions: A non-stationary view,” in *Proc. Innov. Appl. Artif. Intell. Conf.*, vol. 33, pp. 1182–1189, 2019.
- [54] R. Bassily, A. Smith, and A. Thakurta, “Private empirical risk minimization: Efficient algorithms and tight error bounds,” in *2014 IEEE 55th Annu. Symp. Found. Compute. Sci.*, pp. 464–473, IEEE, 2014.
- [55] X. Chen, S. Z. Wu, and M. Hong, “Understanding gradient clipping in private SGD: A geometric perspective,” *Adv. Neural Inf. Process. Syst.*, vol. 33, 2020.
- [56] N. Palleit and T. Weber, “Time prediction of non flat fading channels,” in *2011 IEEE Int. Conf. Acoust. Speech Signal Process. (ICASSP)*, pp. 2752–2755, IEEE, 2011.
- [57] H. Kim, S. Kim, H. Lee, C. Jang, Y. Choi, and J. Choi, “Massive MIMO channel prediction: Kalman filtering vs. machine learning,” *IEEE Trans. Commun.*, vol. 69, no. 1, pp. 518–528, 2021.
- [58] C. Li, J. Zhang, S. Song, and K. B. Letaief, “Selective uplink training for massive MIMO systems,” in *2016 IEEE Int. Conf. Commun. (ICC)*, pp. 1–6, IEEE, 2016.
- [59] B. Y. Shikur and T. Weber, “Channel prediction using an adaptive kalman filter,” in *WSA 2015, 19th Int. ITG Workshop Smart Antennas*, pp. 1–7, VDE, 2015.
- [60] C.-K. Wen, W.-T. Shih, and S. Jin, “Deep learning for massive MIMO CSI feedback,” *IEEE Wireless Commun. Lett.*, vol. 7, no. 5, pp. 748–751, 2018.
- [61] P. Dong, H. Zhang, G. Y. Li, N. NaderiAlizadeh, and I. S. Gaspar, “Deep CNN for wideband mmwave massive MIMO channel estimation using frequency correlation,” in *2019 IEEE Int. Conf. Acoust. Speech Signal Process. (ICASSP)*, pp. 4529–4533, IEEE, 2019.
- [62] Y. Yang, F. Gao, C. Xing, J. An, and A. Alkhateeb, “Deep multimodal learning: Merging sensory data for massive MIMO channel prediction,” *IEEE J. Sel. Areas Commun.*, vol. 39, no. 7, pp. 1885–1898, 2020.
- [63] Y. S. Can and C. Ersoy, “Privacy-preserving federated deep learning for wearable iot-based biomedical monitoring,” *ACM Trans. Internet Technol. (TOIT)*, vol. 21, no. 1, pp. 1–17, 2021.
- [64] S. Greene, H. Thapliyal, and A. Caban-Holt, “A survey of affective computing for stress detection: Evaluating technologies in stress detection for better health,” *IEEE Cons. Electron. Mag.*, vol. 5, no. 4, pp. 44–56, 2016.
- [65] D. Tse and P. Viswanath, *Fundamentals of wireless communication*. Cambridge university press, 2005.